Groundwater

Structural and Hydrogeological Controls on Hydrocarbon and Brine Migration into Drinking Water Aquifers in Southern New York

by Rebecca L. Kreuzer[1], Thomas H. Darrah[2], Benjamin S. Grove[3], Myles T. Moore[3], Nathaniel R. Warner[4], William K. Eymold[3], Colin J. Whyte[3], Gautam Mitra[1], Robert B. Jackson[5], Avner Vengosh[6], and Robert J. Poreda[1]

Abstract

Environmental concerns regarding the potential for drinking water contamination in shallow aquifers have accompanied unconventional energy development in the Northern Appalachian Basin. These activities have also raised several critical questions about the hydrogeological parameters that control the naturally occurring presence and migration of hydrocarbon gases in shallow aquifers within petroliferous basins. To interrogate these factors, we analyzed the noble gas, dissolved ion, and hydrocarbon gas (molecular and isotopic composition) geochemistry of 98 groundwater samples from south-central New York. All samples were collected $\gg$1km from unconventional drilling activities and sample locations were intentionally targeted based on their proximity to various types of documented fault systems. In agreement with studies from other petroliferous basins, our results show significant correlations between elevated levels of radiogenic [^{4}He], thermogenic [CH_4], and dissolved ions (e.g., Cl, Br, Sr, Ba). In combination, our data suggest that faults have facilitated the transport of exogenous hydrocarbon-rich brines from Devonian source rocks into overlying Upper Devonian aquifer lithologies over geologic time. These data conflict with previous reports, which conclude that hydrodynamic focusing regulates the occurrence of methane and salt in shallow aquifers and leads to elevated levels of these species in restricted flow zones within valley bottoms. Instead, our data suggest that faults in Paleozoic rocks play a fundamental role in gas and brine transport from depth, regulate the distribution of their occurrence in shallow aquifers, and influence the geochemistry of shallow groundwater in this petroliferous basin.

Introduction

The emergence of unconventional energy development from tight shales has catalyzed concerns about the potential for compromised drinking-water quality near areas of shale-gas development (e.g., Osborn et al. 2011; Warner et al. 2012a; Jackson et al. 2013; Molofsky et al. 2013; Brantley et al. 2014; Darrah et al. 2014, 2015b; Vengosh et al. 2014; Warner et al. 2014; Siegel et al. 2015; Humez et al. 2016; Harkness et al. 2017; Nicot et al. 2017a, 2017b, 2017c; Darrah 2018). Fugitive methane contamination has been documented in a subset of wells near drill sites (Osborn et al. 2011; Jackson et al. 2013; Darrah et al. 2014; Heilweil et al. 2015; Sherwood et al. 2016), while others have documented natural methane contamination unrelated to shale gas development (Warner et al. 2013; Molofsky et al. 2013; Baldassare et al. 2014; Darrah et al. 2015b; Siegel et al. 2015; Harkness et al. 2017; Eymold et al. 2018).

In the Northern Appalachian Basin (NAB), these questions and concerns have led to a massive effort to establish and understand the baseline water chemistry and hydrogeology of shallow drinking-water aquifers,

[1]Department of Earth and Environmental Sciences, University of Rochester, 227 Hutchison Hall, Rochester, NY 14627; rkreuzer@ur.rochester.edu; gautam.mitra@rochester.edu; poreda@earth.rochester.edu

[2]Corresponding author: Divisions of Solid Earth Dynamics and Water, Climate and the Environment, School of Earth Sciences, The Ohio State University, 125 South Oval Mall, Columbus, OH 43210; darrah.24@osu.edu

[3]Divisions of Solid Earth Dynamics and Water, Climate and the Environment, School of Earth Sciences, The Ohio State University, 125 South Oval Mall, Columbus, OH 43210; grove.139@osu.edu; moore.3222@osu.edu; eymold.1@osu.edu; whyte.25@osu.edu

[4]Department of Civil and Environmental Engineering, Pennsylvania State University, Sackett Building, 212 East College Avenue University Park, PA 16802; nrw6@psu.edu

[5]School of Earth, Energy, and Environmental Sciences, Woods Institute for the Environment, and Precourt Institute for Energy, Stanford University, Y2E2 Building Stanford, CA 94305; rob.jackson@standford.edu

[6]Division of Earth and Ocean Sciences, Nicholas School of the Environment, Duke University, 205 Old Chemistry Building Durham, NC 27708; vengosh@duke.edu

Article impact statement: We examine the baseline water quality, occurrence, and hydrogeological context of naturally occurring methane and salts in southern New York.

Received December 2017, accepted December 2017.

doi: 10.1111/gwat.12638

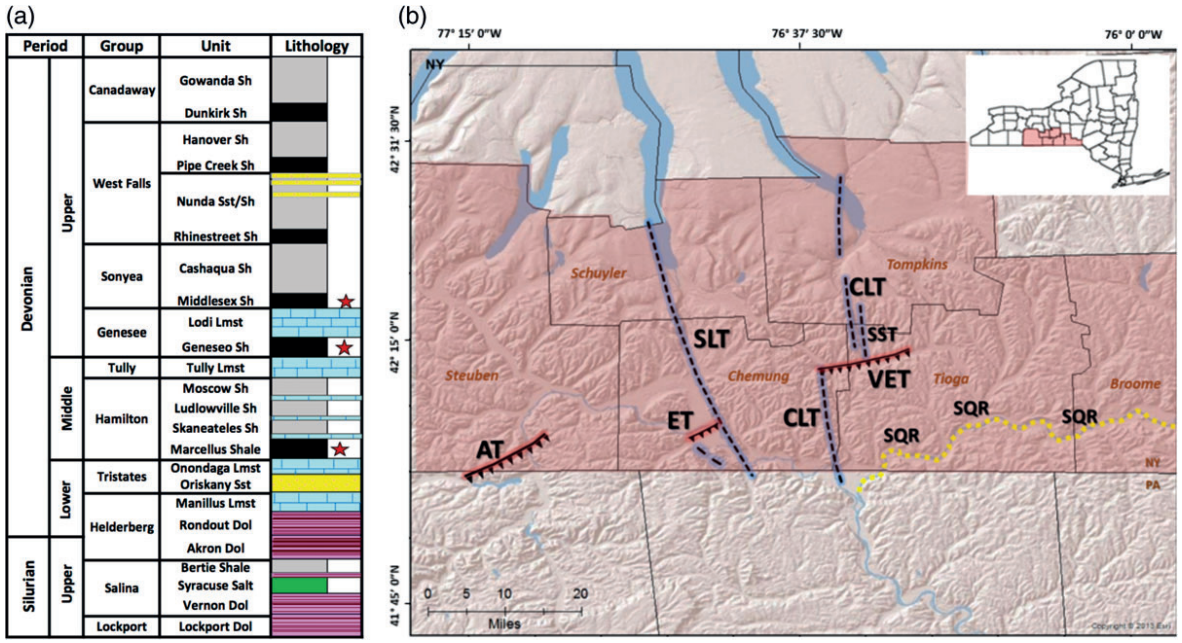

Figure 1. (a) Generalized stratigraphic column of New York. Red stars indicate known or potential gas- or brine-producing horizons. (b) Geographic location of the study area and documented fault systems. The ~N-S striking tear faults (blue/black dashed lines) include: Seneca Lake tear (SLT) fault, Cayuga Lake tear (CLT) fault, and Sulphur Springs suspected-tear (SST) fault. Thrust faults strike ~NE-SW (pink/black lines) and include: Addison thrust (AT) fault, Elmira thrust (ET) fault, and Van Etten thrust (VET) fault. Yellow dashed line represents the Susquehanna River trend (SQR).

the distribution of naturally occurring hydrocarbon gases and diluted brines, and to identify any potential drilling-associated environmental risks. Still, the hydrogeological factors that control the presence and migration of methane and higher order aliphatic hydrocarbons (ethane, propane, etc.) in shallow aquifers remain somewhat controversial and relatively poorly understood (Osborn et al. 2011; Warner et al. 2012a; Jackson et al. 2013; Molofsky et al. 2013; Vengosh et al., 2014; Darrah et al. 2015a, 2015b; Harkness et al. 2017, 2018; Darrah 2018). Some critical remaining questions include: What is the geochemical character of naturally occurring methane and other hydrocarbon gases? What information can the geochemistry of hydrocarbon- and salt-rich fluids tell us about the migration of these contaminants to shallow aquifers? Do geological structures lead to predictable patterns for the occurrence of natural hydrocarbon gases and brines? Do hydrocarbon gases and brines occur at elevated levels in valley-bottom aquifers as a function of hydrodynamic focusing or are they instead transmitted preferentially along deformational features underlying valley bottoms (e.g., tear faults, thrust faults, fold-accommodation faults)?

In other parts of the NAB, such as northeastern Pennsylvania and West Virginia, water (e.g., Cl, Br, Sr., Ba, Br/Cl, $^{87}Sr/^{86}Sr$, Ba/Sr) and gas geochemistry (e.g., [CH_4], C_2+/C_1, [^4He], $^4He/CH_4$, $^{20}Ne/^{36}Ar$, $\delta^{13}C$-CH_4) have been used to determine the genetic source(s) of natural gas and salts, documenting the presence of exogenous hydrocarbon- and salt-rich fluids in Upper Devonian (UD) aquifers, establish a relationship between the occurrence of hydrocarbon- and salt-rich fluids and valley bottoms/structural features, and establish a baseline geochemical character on which to differentiate stray gases (Warner et al. 2012a; Darrah et al. 2014, 2015b; Siegel et al. 2015; Harkness et al. 2017).

Similarly, studies that include groundwater data from the state of New York demonstrate the presence of elevated levels of combustible hydrocarbon gases unrelated to shale-gas development (Williams 1998; Heisig and Scott 2013). These studies suggest that naturally occurring, elevated hydrocarbon gas concentrations tend to occur in localized valley bottoms consistent with reports from Pennsylvania and West Virginia (Williams et al. 1998; Warner et al. 2012a; Jackson et al. 2013; Molofsky et al. 2013; Darrah et al. 2014, 2015b; Siegel et al. 2015; Harkness et al. 2017). The occurrence of elevated hydrocarbon gas concentrations in valley bottoms has been interpreted to occur in confined aquifers as the result of natural hydrodynamic flow processes that have flushed the gas- and salt-rich waters from the "uplands" and focused them into restricted flow zones in the valley bottoms (Taylor 1984; Williams et al. 1998; Heisig and Scott 2013; Molofsky et al. 2013; Siegel et al. 2015; Harkness et al. 2017).

The process of hydrocarbon gas and brine migration along faults and zones of intense fracturing has also been widely documented in the literature (Evans 1995; Caine et al. 1996; Jacobi 2002; Moritz et al. 2015; Harkness et al. 2017, 2018; Eymold et al. 2018). Although south-central New York is often considered structurally featureless, consisting only of a gently southward-dipping sequence of broadly folded anticlines, the area contains many well-documented zones of regional-scale faults.

Examples include approximately N-S trending strike-slip fault systems (e.g., Cayuga Lake and Seneca Lake "tear" faults) and other approximately NE-SW trending thrust faults (e.g., Van Etten, Elmira, and Addison thrust faults; Figure 1) (Fettke 1954; Frey 1973; Murphy 1981). Therefore, in addition to hydrodynamic flow processes, faults may also affect the distribution of hydrocarbon gases and brines in shallow aquifers as documented in other areas within the NAB (Moritz et al. 2015; Darrah et al. 2015b; Harkness et al. 2017). Nonetheless, there have been relatively few studies that have examined the potential relationships between hydrocarbon- and salt-rich fluids in shallow aquifers and faults in this area, or more broadly within other petroleum basins.

Here, we examine the groundwater geochemistry of shallow aquifers in the southern tier of New York State. Specifically, we interrogate the geospatial patterns and mechanisms of hydrocarbon gas and brine contamination in shallow aquifers with respect to known and mapped geological structures. To accomplish this, we examine a suite of geochemical tracers (i.e., dissolved inorganic ions, the molecular and isotopic composition of hydrocarbons, and noble gas elemental abundances and their isotopes) that have proven to be effective tracers of crustal fluid migration in other locations within the NAB and elsewhere (Warner et al. 2012a; Jackson et al. 2013; Darrah et al. 2014, 2015a, 2015b; Wen et al. 2016; Harkness et al. 2017, 2018; Eymold et al. 2018).

As part of this study, we collected water samples from groundwater wells across six counties of south-central New York (Broome, Chemung, Schuyler, Steuben, Tioga, and Tompkins) (Figure 1). This study area was chosen for two reasons: (1) it is an area that is actively being prospected for hydrocarbon extraction from the "Marcellus Fairway" and thus provides a timely opportunity to establish accurate baseline hydrogeological conditions in an area of potential shale gas development, albeit within an area with a history of conventional energy development and (2) faults have previously been documented and studied within this region (Wedel 1932; Finn 1949; Fettke 1954; Frey 1973; Murphy 1981; Jacobi 2002). The presence of documented faults within this region provides a ready opportunity to examine the relationship between faults and water and gas geochemistry in a relatively simplistic geological setting.

Geological Setting

Geologic Overview of the NAB

The NAB is an archetypal foreland basin in the northeastern United States. Like all sedimentary basins, the tectonic history of the NAB plays a fundamental role in the generation, migration, and emplacement of hydrocarbons and brines within this region. Significant oil and gas production occurs within various lithologies throughout the NAB, including underneath the southern tier of New York.

Lithologies of interest in this study area include the Middle Ordovician Trenton/Black River Group, the Upper Silurian Salina Formation, the Middle Devonian Hamilton Group, and various UD formations described in more detail below. Hydrocarbon production is dominated by two genetic groups: (1) Middle Devonian and (2) Ordovician black shales that produce hydrocarbons of varying thermal maturity according to the maximum burial depth of formations locally (e.g., Ryder and Zagorski 2003). A more detailed summary of hydrocarbon potential is included below.

The Taconic Orogeny produced a series of interbedded limestones and shales known as the Trenton/Black River Group and later, the overlying organic-rich Utica shale (Milici and Witt 1988). The Salina Formation served as the regional decollement along which deformation occurred during the Alleghanian orogeny. The Salina Formation consists of interbedded shales, dolomites, and major, laterally extensive evaporite deposits (Frey 1973; Scanlin and Engelder 2003). The thick Salina evaporites acted as a barrier to fluid flow between the overlying (e.g., UD) and underlying (e.g., Silurian and Ordovician) rock units (Drozd and Cole 1994; Ryder et al. 1998) and prevented deformation features below the decollement (i.e., Ordovician and Silurian formations) from influencing the deformation style or hydraulic connectivity of the Devonian formations relevant to this study (Frey 1973; Scanlin and Engelder 2003). Thus, herein, we confine our interpretation to the lithologies within the Hamilton Group and subsequent hydrocarbon generation and migration in the Devonian sedimentary sequences of the southern tier of New York.

The Middle Devonian Hamilton Group is a wedge of marine sediments that thickens to the east and south, which includes the organic- and siliciclastic-rich, regionally extensive Marcellus Fm. at its base (Figure 1). The Marcellus Fm. overlies the Lower Devonian Oriskany sandstone and Onondaga limestone (Ryder et al. 1996; Straeten et al. 2011). Marcellus conodont alteration index, (CAI) values above 3 and vitrinite reflectance (% R_o) values above 2 in the area correlate well with the postmature, dry natural gas that is produced from the Marcellus Fm. in this area (Repetski et al. 2008). The black, organic-rich sediments of the Marcellus interfinger with limestone units and grade into the gray shales or mudstones of the remaining Hamilton Group. The Tully Limestone lies immediately above the Hamilton Group (Frey 1973).

The UD formations consist of thick synorogenic deposits including some organic-rich black shale units such as the Geneseo, Middlesex, Rhinestreet, Pipe Creek, and Dunkirk (David et al. 2004), which overlie the Tully Limestone. Heterogeneities in total organic carbon (TOC), thermal maturity, and thickness cause these shales to have highly variable production potential across the NAB (Repetski et al. 2008). In our study area, the Geneseo black shale is a thick (25 to 45 m), mature to postmature source of natural gas with thermal maturation isograds that closely mimic the Marcellus (Hill and Lombardi 2002). Although there is little TOC or thermal maturity data on

the Middlesex Shale, it is also a potential source of UD natural gas in the area, especially in Tioga County (Hill and Lombardi 2002). The organic-rich Rhinestreet, Pipe Creek, and Dunkirk black shales are all major, thermally mature UD source rocks throughout much of the western Appalachian Basin (Milici and Witt 1988). However, in our study area, these units have mostly graded into gray shales that have been diluted by clastic materials (Hill and Lombardi 2002) and are therefore not likely significant sources of natural gas in the region.

Structural Overview of the NAB

The earliest attempts to understand the geology of New York State documented two important features within our study area: (1) anticlines are "doubly plunging," creating structural domes and saddles along their length and (2) anticlinal trends abruptly change direction in groups along N-NW trending lineaments (Wedel 1932). Later, Finn (1949) showed that the major anticlinal trends coincide with the prominent changes in fold trends reflecting tear-faulting (i.e., strike-slip faulting) that occurred along the margins of semi-independently advancing blocks (Figure 1; Jacoby and Dellwig 1974; Murphy 1981).

Alleghanian thin-skinned tectonics in the Appalachian Plateau brought about the N-NW transport of the semi-independently advancing blocks via bedding-plane slip along the basal decollement located in the salt-bearing Upper Silurian Salina Group (Rodgers 1949). The tear faults that bound these fault blocks are *primary* tear faults (formed before folding) that likely remained active throughout the Alleghanian Orogeny (Dahlstrom 1970). They can strike either transverse (i.e., N-S or NNW-SSE) or oblique to the regional anticlinal trend (i.e., NNE-SSW).

This N-NW translation of the NAB Devonian sediments occurred almost exclusively above the basal decollement (Faill and Nickelsen 1973; Frey 1973; Hatcher et al. 1989). Progressive deformation led to the formation of concentrically folded, salt-cored anticlines (Faill and Nickelsen 1973; Hatcher et al. 1989). A logical outgrowth of concentric folding is the development of fold-accommodation thrust faulting (Mitra 2002). As an anticline grows, increased tightening creates a "space problem" in the anticlinal core and thrust faults form to facilitate movement of material out of the tightening core. This process can lead to subsurface, graben-like features on the crest of the anticline, and locally, very steeply dipping strata (Mitra 2002). Numerous studies have documented a regional prevalence of symmetrical overthrusting with a resulting "graben" underlying the crest of an anticline (Frey 1973; Murphy 1981). These faults originate from a detachment and offset overlying subsurface structure contours, often including the Tully Limestone (Dahlstrom 1970; Frey 1973; Jacobi 2002). The structures observed in the Lower Devonian strata likely transition into secondary detachment surfaces in overlying, incompetent units (i.e., black shales) of the UD strata and/or die out as splay faults (Frey 1973). However, due to a lack of clear seismic marker beds, much of the UD structure is unknown.

Fold intensity of the Alleghany Plateau generally decreases to the northwest, away from the Appalachian Structural Front (ASF). However, the Sabinsville/Elmira anticline marks a boundary within the Plateau where fold amplitudes drastically decrease, analogous to the ASF (Wedel 1932). This feature, called the Intra-Plateau Structural Front, subdivides the NAB into a High Plateau Province to the south of the Sabinsville/Elmira anticline, and a Low Plateau Province to the north (Gwinn 1964) (Figure 3).

Following Alleghanian tectonics, Triassic rifting of Pangaea along with Pleistocene glacial and post-glacial processes (i.e., valley incision and isostatic rebound) resulted in exhumation of UD formations, which likely increased hydraulic conductivity and facilitated "recent" meteoric recharge of modern UD aquifers (Lerche et al. 1997; Darrah et al. 2015b). More comprehensive considerations of the tectonic history are available elsewhere (Engelder et al. 2009; Lash and Engelder 2009; Burruss and Laughrey 2010), but a summary is included below.

Study Area Information

Hydrogeology

The typical depth of shallow drinking-water wells in our study was 10 to 65 m, while some wells range up to 182 m in depth. Bedrock outcrop and shallow aquifers consist of UD shales and siltstones with some fine-grained sandstones, limestones, and dolostones of the Westfalls or Sonyea Groups (Figure 1). Neotectonic fractures following postglacial rebound provide sufficient permeability for these shallow UD formations to serve as aquifers. In addition to the bedrock aquifers, unconfined valley fill aquifers consist of stratified, Pleistocene-aged sand and gravel deposits and recent alluvial deposits (Miller and Pitman 2012). Thin deposits of low permeability, unstratified glacial till locally form confining layers within the valley fill aquifers and form unconsolidated deposits on bedrock in many upland regions (Miller and Pitman 2012; Heisig and Scott 2013).

Structural Geology

Six regional anticlines trend approximately NE-SW or E-W across the six-county area and two smaller anticlines are present locally in Tioga and Broome counties (Figure 1). The fault systems identified in south-central New York include three thrust faults and two tear faults or en-echelon systems of tear faults (Murphy 1981; Jacobi 2002). Thrust faults include the Addison thrust, Elmira thrust, and Van Etten thrust. All these faults strike parallel to the local trend of the anticlines and correlate in space with anticlinal dome structures. No surface manifestations (e.g., lineaments or valleys) of the Addison thrust have been documented. The Elmira thrust occupies a prominent valley that defines a topographic lineament, while the Van Etten thrust extends eastward from the town of Van Etten to Candor where it terminates (Figure 1).

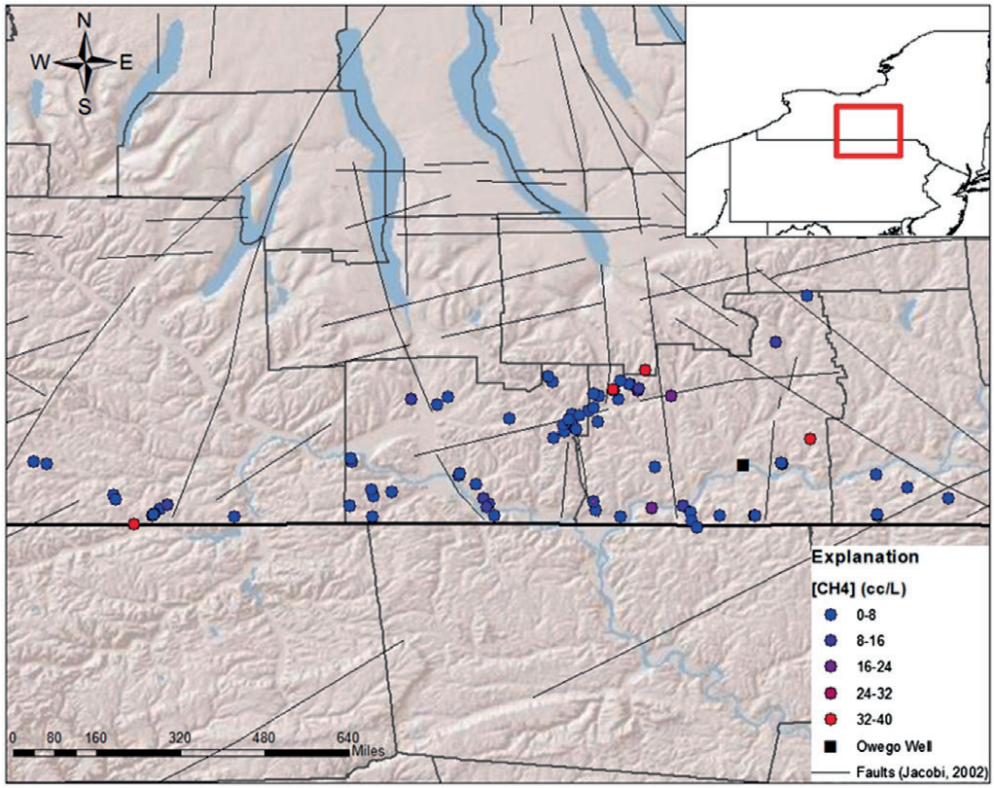

Figure 2. Digital elevation map of groundwater sample locations ($n = 98$) across six counties of south-central New York. Color coding represents dissolved methane concentrations, with purple and red indicating a concentration exceeding U.S. Department of Interior and New York State guidelines for hazard mitigation (14 ccSTP/L or 10 mg/L). The black square represents the location of the Owego brine sample.

Methods

Sample Selection and Classification

We examine the noble gas, hydrocarbon (molecular and stable isotopic [δ^{13}C-CH_4 and δ^{2}H-CH_4]), and dissolved ion (e.g., Cl, Br, Sr., Ba) compositions of groundwater samples collected from 97 domestic water supply wells across Broome, Chemung, Schuyler, Steuben, Tioga, and Tompkins counties of south-central New York and one natural gas-rich brine collected from a geothermal well near Owego, New York (Figure 2). In this study, we intentionally targeted a subset of water wells near previously mapped fault systems and wells from which samples are known to have elevated methane $\gg$1 km from any drilling activities, and other water wells near those with elevated methane levels $\gg$1km from drilling, in order to characterize the hydrogeological context of naturally elevated methane (and salts) throughout the study area. We classify samples as fault-associated and nonfault-associated based on proximity to a mapped fault. Samples within 1 km of a mapped fault are characterized as fault-associated, while those greater than 1 km from a mapped or projected fault trace are characterized as nonfault associated.

Of our 98 samples, we identify 42 as nonfault-associated, and 31 as fault-associated, and 26 additional samples that have an unclassified relationship with respect to faulting. Fault locations based on the Wedel (1932) map (Figure 1) are plotted on the ArcGIS version 12.0 DEM maps downloaded from the ArcGIS world imagery online database and projected in the WGS 1984 coordinate system using ArcGIS 12.0.

Sampling Methods and Analysis

All samples ($n = 98$) were collected and analyzed using standard methods reported previously. Before sampling, wells were purged for at least 30 min to remove stagnant water and simultaneously monitored for pH, electrical conductance, and temperature until stable values were obtained. Water samples were collected prior to any treatment systems and were filtered and preserved following USGS protocols (USGS 2011). The methods for the analysis of inorganic constituents were identical to those reported previously in this volume (Harkness et al. 2018). The methods for the analysis of major gases and noble gases were also identical to those reported previously (Darrah et al. 2013; Kang et al. 2016; Moore et al. 2018; Eymold et al. 2018).

The stable carbon isotopic composition of methane (δ^{13}C-CH_4) was determined for all samples with [CH_4] exceeding 0.5 ccSTP/L ($n = 57$). Dissolved hydrocarbon gas samples were collected in the field using procedures detailed by Isotech Laboratories (Isotech 2011), stored on ice until delivery to their facilities, and analyzed for methane, ethane, and propane concentrations as well as isotopic compositions of methane. Procedures for gas

Table 1
Major Dissolved Ions

Sample ID	[Sr] mg/L	[Ba] μg/L	[Cl] mg/L	[Br] mg/L	[Na] mg/L	Br/Cl
NY-01	0.159	37	3.44	—	6.13	—
NY-02	0.151	304	0.83	0.009	7.77	1.06×10^{-2}
NY-03	0.224	156	41.07	0.150	13.21	3.70×10^{-3}
NY-04	1.948	91	159.40	0.098	50.29	6.00×10^{-4}
NY-05	1.275	148	4.45	0.024	30.93	5.50×10^{-3}
NY-06	0.902	30	5.83	0.037	35.78	6.41×10^{-3}
NY-07	0.260	24	1.66	0.017	27.71	1.02×10^{-2}
NY-08	1.014	52	—	—	54.64	—
NY-09	0.016	11	108.40	0.157	114.99	1.45×10^{-3}
NY-10	0.302	47	—	—	90.81	—
NY-11	0.126	238	137.20	0.037	48.25	2.67×10^{-4}
NY-12	0.101	49	1.57	0.007	11.46	4.60×10^{-3}
NY-13	0.056	48	10.59	0.010	5.50	9.86×10^{-4}
NY-14	0.180	106	1.10	0.007	18.26	6.34×10^{-3}
NY-15	0.525	130	0.80	0.006	10.67	7.05×10^{-3}
NY-16	0.345	132	52.24	0.026	7.92	4.99×10^{-4}
NY-17	0.627	262	20.48	0.018	27.25	9.02×10^{-4}
NY-18	0.122	86	51.90	0.017	89.13	3.28×10^{-4}
NY-19	1.246	1412	172.98	1.259	133.90	7.30×10^{-3}
NY-20	0.172	115	2.36	0.008	6.45	3.30×10^{-3}
NY-23	1.240	760	190.00	5.400	136.87	2.84×10^{-2}
NY-24	1.181	133	54.00	1.500	124.81	2.78×10^{-2}
NY-25	1.245	39	29.00	0.800	52.28	2.76×10^{-2}
NY-26	0.749	49	180.00	5.100	62.90	2.83×10^{-2}
NY-27	1.315	1176	184.00	5.200	120.95	2.83×10^{-2}
NY-28	0.526	122	31.00	0.020	87.15	6.45×10^{-4}
NY-29	0.133	28	138.00	—	43.99	—
NY-30	1.014	54	32.00	—	15.33	—
NY-31	0.513	95	—	0.100		—
NY-32	0.385	141	20.80	1.700	63.41	4.81×10^{-3}
NY-33	0.566	230	197.20	—	38.50	8.62×10^{-3}
NY-34	0.794	702	143.00	0.009	81.10	6.29×10^{-5}
NY-35	0.412	597	23.00	0.005	97.11	2.17×10^{-4}
NY-36	0.563	332	27.00	0.010	70.96	3.70×10^{-4}
NY-38	0.411	667	55.75	0.250	118.78	4.48×10^{-3}
NY-50	3.152	2813	313.45	1.080	147.48	3.45×10^{-3}
NY-51	0.011	3	7.52	—	6.50	—
NY-52	0.031	86	14.98	—	18.52	—
NY-53	0.010	4	2.25	—	4.66	—
NY-54	1.673	3047	346.80	0.510	65.67	1.47×10^{-3}
NY-55	0.906	369	3.37	0.005	55.87	1.48×10^{-3}
NY-56	—	84	3.92	0.567	26.44	1.45×10^{-1}
NY-57	0.084	21	10.30	0.936	12.57	9.08×10^{-2}
NY-58	0.328	190	29.51	0.041	25.79	1.38×10^{-3}
NY-59	0.576	60	9.14	0.257	77.35	1.40×10^{-3}
NY-60	0.126	94	—	—	1.34	—
NY-61	—	1	14.27		50.67	—
NY-62	0.447	57	7.11	0.137	26.96	1.93×10^{-2}
NY-63	0.668	41	—	—	19.76	—
NY-64	1.025	68	25.76	—	20.21	—
NY-65	0.688	333	297.99	6.619	13.07	2.22×10^{-2}
NY-66	0.090	25	—	—	3.87	—
NY-67	0.458	93	3.81	0.124	59.10	3.25×10^{-2}
NY-68	0.274	384	66.51	0.050	6.71	7.52×10^{-4}
NY-69	0.580	141	1.77	0.009	11.29	5.30×10^{-3}
NY-70	0.262	94	1.60	—	13.49	—
NY-71	0.021	5	0.69	—	1.92	—
NY-72	0.293	769	57.85	0.642	41.94	1.11×10^{-2}

Table 1
Continued

Sample ID	[Sr] mg/L	[Ba] μg/L	[Cl] mg/L	[Br] mg/L	[Na] mg/L	Br/Cl
NY-73	0.104	131	39.80	0.105	69.20	2.64×10^{-3}
NY-74	0.080	241	168.13	—	15.38	—
NY-75	0.075	86	18.45	—	11.90	—
NY-76	0.407	159	14.35	0.220	36.55	1.54×10^{-2}
NY-77	0.324	117	1.26	0.022	7.61	1.75×10^{-2}
NY-78	0.076	533	85.44	0.010	68.05	1.17×10^{-4}
NY-79	0.670	67	—	—	19.39	—
NY-80	0.493	533	82.10	2.352	46.55	2.87×10^{-2}
NY-81	0.670	1732	214.16	5.562	35.21	2.60×10^{-2}
NY-86	1.073	1182	62.42	1.376	65.43	2.20×10^{-2}
NY-88	1.100	419	376.04	1.568	—	4.17×10^{-3}
NY-89	0.400	135	68.94	0.068	—	9.82×10^{-4}
NY-90	0.689	307	94.04	0.270	—	2.88×10^{-3}
NY-91	0.257	121	67.94	0.260	—	3.83×10^{-3}
NY-92	1.185	275	387.44	1.215	—	3.13×10^{-3}
NY-94	0.874	246	316.99	1.046	—	3.30×10^{-3}
NY-95	0.419	182	50.04	0.125	—	2.49×10^{-3}
NY-96	0.378	146	61.01	0.140	—	2.30×10^{-3}
NY-97	0.603	217	87.05	0.314	—	3.61×10^{-3}
NY-98	0.876	243	303.14	0.701	—	2.31×10^{-3}
NY-99	0.234	53	21.18	0.068	—	3.21×10^{-3}
NY-100	0.096	40	27.54	0.059	—	2.13×10^{-3}
NY-101	0.101	45	37.45	0.042	—	1.11×10^{-3}
NY-102	0.214	84	34.16	0.068	—	1.98×10^{-3}
NY-103	0.234	76	26.44	0.074	—	2.80×10^{-3}
NY-104	0.371	198	73.05	0.674	—	9.23×10^{-3}
NY-105	0.194	43	23.65	0.042	—	1.77×10^{-3}
NY-106	0.184	61	29.05	0.057	—	1.98×10^{-3}
NY-107	0.704	299	214.05	0.571	—	2.67×10^{-3}
NY-108	0.207	67	19.54	0.075	—	3.81×10^{-3}
NY-109	0.175	51	28.04	0.095	—	3.40×10^{-3}
NY-110	0.177	35	29.14	0.049	—	1.67×10^{-3}
NY-111	0.204	41	37.14	0.075	—	2.03×10^{-3}
NY-112	0.196	29	18.14	0.090	—	4.98×10^{-3}
NY-114	1.051	316	339.04	1.304	—	3.85×10^{-3}
NY-115	0.438	188	131.37	1.048	—	7.98×10^{-3}
NY-116	0.503	234	135.05	0.764	—	5.66×10^{-3}
NY-117	0.206	110	135.66	0.796	—	5.87×10^{-3}
Owego	0.130	121000	13100	112.0	—	8.55×10^{-3}
Min	0.010	1	0.69	0.005	1.336	6.29×10^{-5}
Max	3.152	121,000	13, 100	112.0	147.480	1.45×10^{-1}
Mean	0.514	1520	225.09	2.132	44.652	9.81×10^{-3}
Standard deviation	0.491	12267	1376	12.677	38.657	1.99×10^{-2}

analyses were summarized previously (Osborn et al. 2011; Jackson et al. 2013). Isotech Laboratories used chromatographic separation followed by combustion and dual-inlet isotope ratio mass spectrometry to measure dissolved gas concentrations and δ^{13}C-CH_4 (detection limits for C_1, C_2, and C_3 were 0.001, 0.0005, and 0.0001 mol%, respectively or 1×10^{-5} (ccSTP/L), 5×10^{-6} (ccSTP/L), and 1×10^{-6} (ccSTP/L), respectively). The δ^{13}C-CH_4 values are expressed in per mille (designated hereafter as ‰) vs. the international standard Vienna Peedee belemnite (VDPD), with a standard deviation of ±0.1‰.

The abundance and isotopic composition of noble gases were determined either using a VG 5400 MS at the University of Rochester Rare Gas Laboratory or a Thermo Fisher Helix SFT at The Ohio State University Noble Gas Laboratory following methods reported previously (Darrah and Poreda 2012; Darrah et al. 2013; Moore et al. 2018). The average external precisions based on "known-unknown" standards were all less than ±1.54% for noble gas concentrations with values reported in parentheses (^{4}He [0.87%], ^{22}Ne [1.54%], and ^{40}Ar [0.49%]). These values were determined by measuring referenced

and cross-validated laboratory standards, including an established atmospheric standard (Lake Erie Air) and a series of synthetic natural gas standards obtained from Praxair, including known and validated concentrations of CH_4 to C_5H_{12} hydrocarbons, N_2, CO_2, H_2, O_2, and each of the noble gases. Noble gas isotopic standard errors were approximately ±0.0094 times the ratio of air (or 1.301×10^{-8}) for $^3He/^4He$ ratio, less than ±0.457% and ±0.713% for $^{20}Ne/^{22}Ne$ and $^{21}Ne/^{22}Ne$, respectively, and less than ±0.606 and ±0.439% for $^{38}Ar/^{36}Ar$ and $^{40}Ar/^{36}Ar$, respectively (higher than typical because of interferences from C_3H_8 on mass = 36 and 38).

Statistical Treatment of Data

All maps and well coordinates are plotted using ArcMap GIS 12.0. All graphics are plotted using Sigma Plot 12.3. Statistical evaluations including mean, minima, maxima, standard deviation, and Pearson correlations were performed using SPSS v. 24. Correlation coefficients, r^2, reported in the text were calculated as Pearson's correlation coefficients, and corresponding p values, are provided throughout the text.

We present data from this study with color-coded symbols based on the abundance of methane, where low methane concentrations close to 0 ccSTP/L are blue and range up to red for methane concentrations of 40 ccSTP/L (i.e., the level of methane saturation in groundwater at 10 °C). Data from previous studies are identified by empty green shapes which reflect the source of the data as described in figure caption legends.

Results

Dissolved Ion Chemistry

Groundwater Types

Elevated salt concentrations (e.g., Cl, Br, Ba, and Sr), as well as isotopic (e.g., $^{87}Sr/^{86}Sr$) and molecular ratios (e.g., Ba/Cl, Br/Cl) have been widely used as indicators of brine addition to freshwater aquifers (Warner et al. 2012a; Harkness et al. 2017, 2018). Previous groundwater classification schemes (Warner et al. 2012a; Harkness et al. 2017, 2018) divided water samples according to their salinity, Br/Cl ratios (relative to the seawater value of 0.001), and other major anion compositions (e.g., Cl, HCO_3, SO_4).

In the current study, chloride measurements were obtained for 36 of the 42 nonfault-associated samples. The majority of these samples (26 out of 36) have Cl concentrations less than 20 mg/L with an average of 24.9 mg/L. By comparison, chloride measurements were obtained for all 31 of the fault-associated groundwater samples. Of these samples, 28 have Cl concentrations greater than 20 mg/L and as a group have an average of 121.0 mg/L of Cl. The abundance of Br, Na, and Sr correlate positively with Cl. As a result, there are similar variations between the levels of these elements according to fault-associated or nonfault-associated samples (Table 1).

We find no strong statistical correlation between dissolved Cl, Sr, or Br concentrations with topographic position (i.e., p = 0.08, 0.99, and 0.50, respectively), although a correlation with elevated [Ba] and wells located in valley bottoms (p = 0.03) was identified. Additionally, p-values for dissolved salts with respect to proximity to oil or gas wells are all greater than 0.1, suggesting that the legacy of industrial practices/drilling has had no statistically resolvable effect on inorganic groundwater chemistry in this region.

Hydrocarbon Gases

Hydrocarbon Concentrations and Distribution

Methane concentrations in groundwater from the study area range from below detection limits (b.d.l.) (~0.01 ccSTP/L) to 34.55 ccSTP/L, while the Owego brine sample displayed oversaturated (232.8 ccSTP/L) levels of methane at least partially caused by gas-liquid phase separation (Table 2). The upper limit of 34.55 ccSTP/L is near saturation conditions for methane in fresh water (37.3 ccSTP/L at one atmosphere, at an elevation of 400 m, and at 12 °C). Ethane concentrations were commonly below detection limits, but when detectable, narrowly exceeded 0.001 ccSTP/L. As a result, the C_1/C_2+ ranges from 613 to 11,350 throughout the study. Propane was below detection limits in all of our samples.

Methane concentrations and the C_1/C_2+ did vary accordingly to distance from faults. In the nonfault-associated groundwater samples, only 17 out of 42 samples displayed detectable methane concentrations (Table 2). Of these samples with detectable methane levels, only two displayed methane concentrations above 1.0 ccSTP/L (Table 2). In this subset of samples, the average methane concentration was 0.63 ccSTP/L (Table 2). By comparison, methane was quantifiable in 26 out of 31 fault-associated samples and above 1.0 ccSTP/L in 18 of those 26 samples. The fault-associated samples had average methane concentrations of 10.45 ccSTP/L, excluding the fault-associated oversaturated Owego brine sample. The C_1/C_2+ ratios in nonfault-associated samples ranged from 5814 to 11,350 with an average of 7593, while the C_1/C_2+ ratios in fault-associated samples ranged from 613 to 8403 with an average of 4290. These data indicate that fault-associated samples display both higher levels of methane and, although ethane is relatively low in all samples, relatively higher proportions of ethane (Table 2; Figure 3).

Stable Isotopes of Hydrocarbons

Stable isotopic values of carbon in methane (e.g., $\delta^{13}C\text{-}CH_4$) were measured for 63 of the 98 samples, including 15 nonfault-associated samples and 25 fault-associated samples with CH_4 concentrations that exceed 0.1 ccSTP/L. The $\delta^{13}C\text{-}CH_4$ for these samples show great variability ranging from −34.71‰ to −78.3‰ (Figure 5; Table 2). These values suggest major contributions from biogenic methane in the majority of samples, but display

Table 2
The Molecular and Isotopic Composition of Hydrocarbon Gases

Sample ID	CH_4 ccSTP/L	C_2H_6 ccSTP/L	N_2 ccSTP/L	$\delta^{13}C$-C_1 per mille (‰)	C_1/C_{2+}
NY-01	b.d.l.	b.d.l.	15.70	—	—
NY-02	b.d.l.	b.d.l.	12.96	—	—
NY-03	b.d.l.	b.d.l.	11.55	—	—
NY-04	b.d.l.	b.d.l.	15.05	—	—
NY-05	0.12	b.d.l.	15.71	—	—
NY-06	0.02	b.d.l.	20.04	—	—
NY-07	0.02	b.d.l.	18.69	—	—
NY-08	b.d.l.	b.d.l.	17.46	—	—
NY-09	b.d.l.	b.d.l.	15.33	—	—
NY-10	b.d.l.	b.d.l.	16.65	—	—
NY-11	b.d.l.	b.d.l.	14.52	—	—
NY-12	b.d.l.	b.d.l.	16.38	−43.20	—
NY-13	b.d.l.	b.d.l.	14.51	−43.25	—
NY-14	b.d.l.	b.d.l.	14.69	—	—
NY-15	b.d.l.	b.d.l.	14.29	—	—
NY-16	b.d.l.	b.d.l.	14.51	−34.71	—
NY-17	b.d.l.	b.d.l.	12.89	—	—
NY-18	b.d.l.	b.d.l.	13.37	—	—
NY-19	32.53	b.d.l.	7.08	−63.90	—
NY-20	b.d.l.	b.d.l.	13.45	—	—
NY-23	25.23	b.d.l.	8.82	−40.10	—
NY-24	2.56	b.d.l.	13.41	−37.50	—
NY-25	2.25	b.d.l.	17.07	—	—
NY-26	b.d.l.	b.d.l.	15.06	—	—
NY-27	13.68	b.d.l.	18.04	−45.20	—
NY-28	8.15	b.d.l.	13.22	−47.10	—
NY-29	0.02	b.d.l.	14.89	—	—
NY-30	b.d.l.	b.d.l.	15.27	—	—
NY-31	b.d.l.	b.d.l.	14.23	—	—
NY-32	b.d.l.	b.d.l.	14.38	—	—
NY-33	b.d.l.	b.d.l.	27.54	—	—
NY-34	0.80	b.d.l.	14.82	−53.90	—
NY-35	2.50	b.d.l.	15.81	−78.30	—
NY-36	0.26	b.d.l.	—	−69.40	—
NY-38	11.43	b.d.l.	10.87	−56.30	—
NY-50	13.35	b.d.l.	18.37	−53.10	—
NY-51	b.d.l.	b.d.l.	12.86	—	—
NY-52	—	—	—	—	—
NY-53	0.01	b.d.l.	16.37	—	—
NY-54	17.35	b.d.l.	11.72	—	—
NY-55	1.34	b.d.l.	22.90	−52.50	—
NY-56	0.02	b.d.l.	16.97	—	—
NY-57	0.02	b.d.l.	27.61	—	—
NY-58	0.04	b.d.l.	12.99	−43.20	—
NY-59	0.33	3.40×10^{-5}	14.53	−51.30	9804
NY-60	b.d.l.	1.10×10^{-5}	8.76	−68.50	9350
NY-61	b.d.l.	b.d.l.	20.53	−52.40	6135
NY-62	0.03	4.20×10^{-6}	32.36	−68.30	7353
NY-63	0.03	b.d.l.	27.29	—	
NY-64	0.02	b.d.l.	12.37	−54.20	6135
NY-65	0.18	3.80×10^{-5}	13.74	−53.80	4695
NY-66	0.02	b.d.l.	12.94	—	
NY-67	0.07	1.10×10^{-5}	14.74	−64.90	6536
NY-68	0.05	1.30×10^{-5}	16.26	−47.10	3846
NY-69	0.03	b.d.l.	—	−59.70	11,351
NY-70	b.d.l.	b.d.l.	—	−71.60	7143
NY-71	b.d.l.	b.d.l.	—	—	
NY-72	19.59	4.49×10^{-3}	9.76	−48.40	4367
NY-73	3.96	5.54×10^{-4}	10.96	−70.60	7143

Table 2
Continued

Sample ID	CH_4 ccSTP/L	C_2H_6 ccSTP/L	N_2 ccSTP/L	δ^{13}C-C_1 per mille (‰)	C_1/C_{2+}
NY-74	0.03	8.46×10^{-6}	20.39	−47.60	3546
NY-75	b.d.l.	b.d.l.		−54.30	7299
NY-76	0.50	8.60×10^{-5}	16.79	−56.90	5814
NY-77	b.d.l.	b.d.l.	14.37	−63.40	6314
NY-78	2.67	3.18×10^{-4}	12.46	−68.30	8403
NY-79	—	—	—	—	—
NY-80	18.70	4.49×10^{-3}	11.23	−52.70	4167
NY-81	15.61	6.32×10^{-3}	13.35	−45.30	2469
NY-86	34.55	1.21×10^{-2}	11.99	−47.90	2857
NY-88	10.55	3.36×10^{-3}	12.17	−46.75	3139
NY-89	32.34	1.00×10^{-2}	11.02	−47.34	3229
NY-90	17.17	6.14×10^{-3}	11.46	−45.20	2765
NY-91	4.69	1.01×10^{-3}	10.69	−43.59	4337
NY-92	36.18	2.58×10^{-2}	12.76	−45.12	749
NY-94	13.24	2.83×10^{-3}	14.67	−44.19	4659
NY-95	0.69	1.80×10^{-5}	14.35	−72.24	38,341
NY-96	0.51	b.d.l.	14.51	−72.44	
NY-97	0.81	7.76×10^{-5}	13.97	—	10,478
NY-98	9.75	2.37×10^{-3}	12.14	−51.53	4105
NY-99	1.79	8.44×10^{-5}	12.89	−70.22	21,204
NY-100	1.41	1.08×10^{-4}	12.63	−69.55	13,026
NY-101	0.36	b.d.l.	14.07	−73.15	
NY-102	0.51	b.d.l.	13.08	−68.47	
NY-103	0.45	1.05×10^{-5}	12.84	−72.15	42,426
NY-104	0.19	6.63×10^{-6}	12.84	—	28,729
NY-105	0.16	b.d.l.	14.32	—	
NY-106	1.49	1.35×10^{-4}	14.30	−57.65	10,986
NY-107	0.10	b.d.l.	15.74	—	—
NY-108	0.05	b.d.l.	14.04	—	—
NY-109	0.26	b.d.l.	13.66	—	—
NY-110	0.17	b.d.l.	14.68	—	—
NY-111	0.31	b.d.l.	12.98	—	—
NY-112	0.31	b.d.l.	13.60	—	—
NY-114	1.79	5.30×10^{-4}	13.86	−43.47	3385
NY-115	1.32	6.46×10^{-5}	11.59	−67.49	20,445
NY-116	9.90	1.67×10^{-3}	11.80	−42.45	5927
NY-117	7.42	1.89×10^{-3}	10.03	−52.14	3937
Owego	232.80	3.80×10^{-1}	14.77	−53.40	613
Min	0.01	6.63×10^{-6}	7.08	−78.30	613
Max	232.80	3.80×10^{-1}	32.36	−34.71	42,426
Mean	9.18	1.45×10^{-2}	14.71	−55.41	8903
Standard deviation	29.05	6.58×10^{-2}	3.97	11.14	9205

b.d.l., below detection limits.

intermediate (∼−50‰) to thermogenic values (>−45‰) in a subset of samples. Importantly, the stable isotopic values of carbon in methane (e.g., δ^{13}C-CH_4) were indistinguishable based on the distance from faults. The nonfault-associated samples yielded an average of −55.46‰, while the fault-associated samples averaged −54.64‰ (Table 2).

We also examined the correlation between methane concentration and isotopic composition with proximity to active or legacy oil/gas wells and topographic positioning in a valley or upland setting, as defined by Heisig and Scott (2013) (Figure 7). We found no significant correlation between CH_4 concentrations and proximity (i.e., >1 km or <1 km) to an oil or gas well ($p = 0.34$). We did identify a correlation between CH_4 concentrations and topographic setting ($p = 0.005$); elevated methane concentrations (i.e., $[CH_4] > 0.1$ ccSTP/L) are observed at lower elevations. This observation is in general agreement with previous findings (Warner et al. 2012a; Heisig and Scott 2013; Molofsky et al. 2013; Siegel et al. 2015; Darrah et al. 2015b; Harkness et al. 2017) in the NAB and is expected based on the overlap between fault-associated and valley

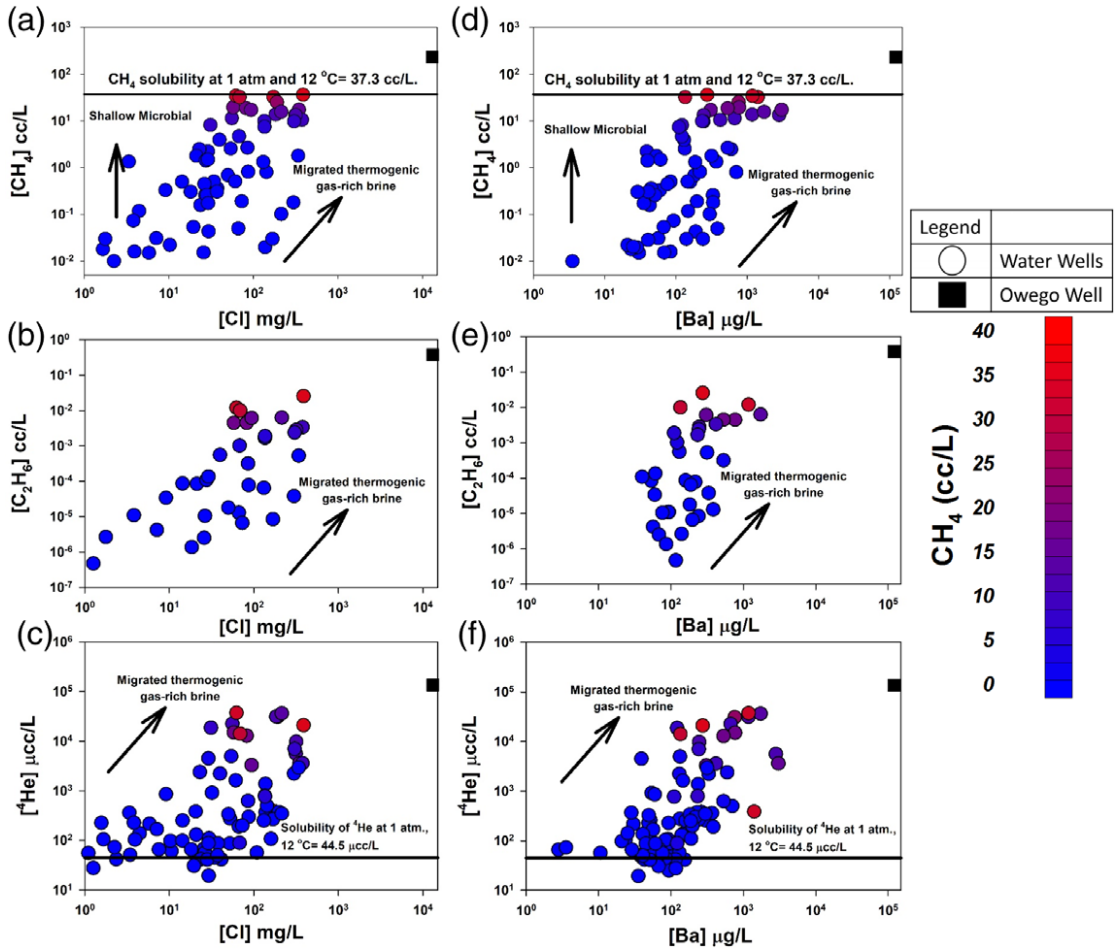

Figure 3. Variations of [CH_4], [C_2H_6], and [^{4}He] compared to [Cl] and [Ba] in groundwater and a natural gas-rich brine (brine collected from Owego, New York shown as a black square) collected from south-central New York. In general, CH_4, C_2H_6, and ^{4}He concentrations increase with concentrations of brine components (e.g., Cl and Ba, or Br [not shown]) across the study area. Notice that the increase in [CH_4] "rolls over" as methane concentrations approach saturation levels for shallow groundwater. The upper level (saturation = 37.3 ccSTP/L at 10°C and 1 atm) for [CH_4] demonstrates how groundwater saturation or "bubble point" limits the maximum dissolved methane concentrations in natural groundwater conditions. The positive correlations of [CH_4], [C_2H_6], and [^{4}He] with [Cl] and [Ba] suggest the coherent migration of a gas-rich, saline fluid from deeper formations into Upper Devonian aquifers across the region that has been recently diluted by meteoric water. The coexistence of CH_4, C_2H_6, and ^{4}He suggests a thermogenic source for the hydrocarbon gases.

bottom samples and nonfault-associated and upland samples.

Noble Gases

Helium

Helium concentrations in our groundwater data set range from below ASW values (25×10^{-6} ccSTP/L, where ASW recharged in this area is anticipated to contain $\sim 43 \times 10^{-6}$ ccSTP/L at 10 °C), up to 0.037 ccSTP/L (Table 3). Combined elevated [^{4}He], high He/Ne, and low ^{3}He/^{4}He ($\sim 0.02 R_A$) unambiguously indicate that the CH_4-rich end-member in groundwater from our study area is dominated by an exogenous source of crustal helium external to the present aquifer lithologies (Figure 7), consistent with other studies from the NAB (Darrah et al. 2014, 2015b; Harkness et al. 2017).

Like other studies, the highest levels of ^{4}He in this study area correspond to the highest concentrations of CH_4, Cl, Br, and Ba (Figure 3; Tables 1–3). These results are broadly consistent with the presence of an exogenous thermogenic methane- and salt-rich fluid in shallow aquifers and suggest a coherent migration process delivered hydrocarbon gases, helium, and salts to the shallow aquifers on unknown timescales.

Like methane concentrations and salts, ^{4}He concentrations are significantly higher on average in fault-associated samples (6784×10^{-6} ccSTP/L) than nonfault-associated samples (1847×10^{-6} ccSTP/L; Table 3). Similarly, the ^{3}He/^{4}He is significantly lower (more crustal) in fault-associated samples on average ($0.228 R_A$ vs. $0.624 R_A$; Table 3). While we do observe a subset of samples with high ^{20}Ne and ^{20}Ne/^{36}Ar in the fault-associated samples, there are no statistically significant differences between the groups (Table 3).

Topographic positioning and proximity to an oil or gas well are also considered with respect to [^{4}He]. Although we note the overlap between valley bottoms

Table 3
The Elemental and Isotopic Composition of Major Gases and Noble Gases

Sample ID	^{4}He $\times 10^{-6}$ ccSTP/L	^{3}He/^{4}He R/R_A	^{20}Ne $\times 10^{-6}$ ccSTP/L	Ne $\times 10^{-6}$ ccSTP/L	^{36}Ar $\times 10^{-6}$ ccSTP/L	Ar ccSTP/L	$CH_4/^{36}$Ar	^{4}He/^{20}Ne	^{4}He/^{36}Ar	^{4}He/CH_4 $\times 10^6$	^{20}Ne/^{36}Ar	N_2/Ar
NY-01	50.7	0.9146	254.4	282.7	1613	0.477	—	0.20	0.031	—	0.158	32.9
NY-02	254	0.2596	275.9	306.5	1404	0.415	—	0.92	0.181	—	0.196	31.2
NY-03	41.3	0.8715	157.2	174.6	1248	0.36	—	0.26	0.033	—	0.126	31.3
NY-04	107	0.6647	298.6	331.8	1560	0.461	—	0.36	0.069	—	0.191	32.7
NY-05	138	0.5709	330.8	367.6	1628	0.481	7.25×10^1	0.42	0.085	1170	0.203	32.7
NY-06	214	0.4321	354.8	394.2	1911	0.565	7.85	0.60	0.112	14267	0.186	35.5
NY-07	105	0.6353	266.0	295.6	1972	0.583	9.13	0.39	0.053	5810	0.135	32.1
NY-08	258	0.3677	373.0	414.5	1615	0.477	—	0.69	0.159	—	0.231	36.6
NY-09	56.3	0.9702	224.9	249.9	1623	0.479	—	0.25	0.035	—	0.139	32.0
NY-10	117	0.8098	311.3	345.9	1596	0.472	—	0.38	0.073	—	0.195	35.3
NY-11	1372	0.0885	431.1	479.0	1454	0.430	—	3.18	0.944	—	0.297	33.8
NY-12	224	0.3757	307.3	341.5	1611	0.476	—	0.73	0.139	—	0.191	34.4
NY-13	60.5	0.9246	241.9	268.8	1370	0.405	—	0.25	0.044	—	0.177	35.9
NY-14	55.1	0.9426	187.2	208.0	1518	0.448	—	0.29	0.036	—	0.123	32.8
NY-15	57.0	0.8681	181.0	201.1	1602	0.473	—	0.31	0.036	—	0.113	30.2
NY-16	274	0.5259	231.8	257.6	1519	0.449	—	1.18	0.180	—	0.153	32.3
NY-17	382	0.2910	174.6	194.0	1359	0.402	—	2.19	0.281	—	0.128	32.1
NY-18	86.2	0.5765	194.7	216.3	1310	0.387	—	0.44	0.066	—	0.149	34.5
NY-19	386	0.0920	85.6	95.2	959	0.283	3.39×10^4	4.51	0.403	12	0.089	25.0
NY-20	41.5	1.0475	170.4	189.4	1319	0.390	—	0.24	0.031	—	0.129	34.5
NY-23	30,655	0.0292	257.8	286.5	970	0.287	2.60×10^4	118.9	31.60	1215	0.266	30.8
NY-24	4945	0.0294	248.0	275.6	866	0.256	2.95×10^3	19.94	5.71	1934	0.286	52.4
NY-25	4488	0.0549	438.8	487.5	1769	0.523	1.27×10^3	10.23	2.536	1997	0.248	32.6
NY-26	324	0.3729	261.2	290.2	1440	0.426	—	1.24	0.225	—	0.181	35.4
NY-27	31,151	0.0343	530.6	589.5	1582	0.468	8.65×10^3	58.71	19.69	2277	0.335	38.6
NY-28	18,572	0.0246	548.8	609.8	1263	0.373	6.45×10^3	33.84	14.70	2279	0.434	35.4
NY-29	366	0.2924	359.6	399.5	1487	0.439	1.34×10^1	1.02	0.246	18388	0.242	33.9
NY-30	913	0.2539	434.0	482.2	1468	0.434	—	2.10	0.622	—	0.296	35.2
NY-31	88.6	1.0789	312.4	347.1	1357	0.401	—	0.28	0.065	—	0.230	35.5
NY-32	130	0.5311	323.5	359.4	1391	0.411	—	0.40	0.093	—	0.233	35.0
NY-33	374	0.4933	862.5	958.3	1993	0.589	—	0.43	0.188	—	0.433	46.8
NY-34	497	0.1539	333.0	370.0	1426	0.422	5.62×10^2	1.49	0.349	620	0.233	35.1
NY-35	2380	0.1571	334.9	372.1	1607	0.475	1.55×10^3	7.11	1.48	954	0.208	33.3
NY-36	—		—	—	—	—	—	—	—	—	—	—
NY-38	22,308		275.9	306.5	1140	0.282	1.00×10^4	80.9	19.57	1953	0.242	38.5
NY-50	5570		322.7	358.6	1250	0.369	1.07×10^4	17.3	4.46	417	0.258	49.7
NY-51	65.6		128.3	142.6	1150	0.340	—	0.51	0.057	—	0.112	37.8
NY-52	—		—	—	—	—	—	—	—	—	—	—
NY-53	72.7		269.0	298.9	1462	0.432	6.84	0.27	0.050	77271	0.184	37.9
NY-54	3592		—	—	971	0.287	1.79×10^4	—	3.70	207	—	40.8
NY-55	360		—	359.6	1662	0.491	8.08×10^2	—	0.216	268	—	46.6
NY-56	103		320.0	355.5	1602	0.473	9.94	0.32	0.064	6476	0.200	35.9
NY-57	97.1		302.9	336.5	1936	0.572	1.15×10^1	0.32	0.050	4369	0.156	48.3
NY-58	109		227.1	252.4	956	0.282	4.51×10^1	0.48	0.114	2524	0.238	46.0
NY-59	854		—	—	1055	0.312	3.13×10^2	—	0.810	2587	—	46.6
NY-60	25.0		102.3	113.7	782	0.231	—	0.24	0.032	—	0.131	37.9
NY-61	98.2		303.8	337.5	2068	0.611	—	0.32	0.048	—	0.147	33.6
NY-62	167		477.3	530.4	3081	0.910	1.00×10^1	0.35	0.054	5382	0.155	35.5
NY-63	135		350.9	389.9	4613	1.363	6.21	0.38	0.029	4705	0.076	20.0
NY-64	67.4		154.2	171.3	846	0.250	1.81×10^1	0.44	0.080	4404	0.182	49.5
NY-65	2208		110.3	122.6	1205	0.356	1.49×10^2	20.0	1.83	12267	0.092	38.6
NY-66	141		—	—	1142	0.337	1.80×10^1	—	0.123	6829	—	38.3
NY-67	225		205.6	228.4	1425	0.421	5.17×10^1	1.09	0.158	3057	0.144	35.0
NY-68	189				1280	0.378	3.90×10^1	—	0.148	3787	-	43.0
NY-69	—		—	—	—	—	—	—	—	—	—	—
NY-70	—		—	—	—	—	—	—	—	—	—	—
NY-71	—		—	—	—	—	—	—	—	—	—	—
NY-72	14,875		636.6	707.4	1541	0.455	1.27×10^4	23.4	9.656	759	0.413	21.4
NY-73	2214		266.3	295.9	1249	0.369	3.17×10^3	8.31	1.772	559	0.213	29.7
NY-74	266		281.7	313.0	1630	0.483	1.84×10^1	0.94	0.163	8869	0.173	42.2
NY-75	—		—	—	—	—	—	—	—	—	—	—
NY-76	251		277.3	252.6	2065	0.610	2.42×10^2	1.10	0.122	502	0.110	27.5
NY-77	28		88.1	97.8	1348	0.398	—	0.31	0.021	—	0.065	36.1
NY-78	627		149.5	166.1	1827	0.540	1.46×10^3	4.20	0.343	235	0.082	23.1
NY-79	—	—	—	—	—	—	—	—	—	—	—	—

Table 3
Continued

Sample ID	^{4}He × 10^{-6} ccSTP/L	^{3}He/^{4}He R/R_A	^{20}Ne × 10^{-6} ccSTP/L	Ne × 10^{-6} ccSTP/L	^{36}Ar × 10^{-6} ccSTP/L	Ar ccSTP/L	$CH_4/^{36}$Ar	^{4}He/^{20}Ne	^{4}He/^{36}Ar	^{4}He/CH_4 ×10^{6}	^{20}Ne/^{36}Ar	N_2/Ar
NY-80	12,793		261.0	290.0	1320	0.390	1.42×10^{4}	49.0	9.69	684	0.198	28.8
NY-81	36,167		549.5	610.5	1503	0.444	1.04×10^{4}	65.8	24.06	2317	0.366	30.0
NY-86	37,091		396.5	440.6	1280	0.378	2.70×10^{4}	93.5	28.98	1074	0.310	31.7
NY-88	3567	0.0208	382.2	422.3	1094	0.325	9.64×10^{3}	9.33	3.26	338	0.350	37.5
NY-89	13,987	0.0256	338.8	374.3	832	0.249	3.89×10^{4}	41.3	16.8	432	0.407	44.2
NY-90	3263	0.0178	144.2	126.2	884	0.265	1.94×10^{4}	28.6	3.69	190	0.129	43.3
NY-91	88.3	0.7135	109.2	120.7	783	0.232	5.98×10^{3}	0.81	0.113	19	0.139	46.0
NY-92	20,824	0.0160	375.7	415.0	985	0.273	3.67×10^{4}	55.4	21.147	576	0.382	46.8
NY-94	9725	0.0218	238.6	263.5	1265	0.379	1.05×10^{4}	40.8	7.69	734	0.189	38.8
NY-95	336	0.3202	259.0	286.2	1119	0.332	6.15×10^{2}	1.30	0.300	488	0.231	43.2
NY-96	1621	0.0321	357.3	394.7	1113	0.332	4.56×10^{2}	4.54	1.46	3195	0.321	43.6
NY-97	298	0.1770	152.7	168.8	1017	0.302	8.00×10^{2}	1.95	0.293	366	0.150	46.3
NY-98	6947	0.0378	176.0	194.3	951	0.285	1.02×10^{4}	39.5	7.30	713	0.185	42.6
NY-99	49.4	0.6844	126.2	139.5	1001	0.297	1.79×10^{3}	0.39	0.049	28	0.126	43.4
NY-100	45.9	1.4202	150.8	166.6	900	0.267	1.57×10^{3}	0.30	0.051	33	0.168	47.3
NY-101	86.5	0.2699	131.3	145.1	944	0.280	3.82×10^{2}	0.66	0.092	240	0.139	50.3
NY-102	44.5	0.9070	144.8	160.0	1017	0.301	4.98×10^{2}	0.31	0.044	88	0.142	43.4
NY-103	55.8	1.0449	182.8	202.0	954	0.283	4.67×10^{2}	0.30	0.058	125	0.192	45.4
NY-104	197	1.1507	184.9	204.4	1148	0.340	1.66×10^{2}	1.07	0.172	1038	0.161	37.8
NY-105	41.5	0.2867	105.4	116.5	979	0.290	1.61×10^{2}	0.39	0.042	263	0.108	49.3
NY-106	87.2	0.2832	137.2	151.6	1204	0.357	1.24×10^{1}	0.64	0.072	59	0.114	40.1
NY-107	345	0.4407	251.3	277.8	1515	0.450	6.70×10^{1}	1.37	0.228	3406	0.166	35.0
NY-108	30.6	1.0194	129.3	142.9	1146	0.339	4.70×10^{1}	0.24	0.027	568	0.113	41.4
NY109	40.9	0.8711	133.7	147.7	1166	0.346	2.22×10^{2}	0.31	0.035	158	0.115	39.5
NY-110	19.4	0.5581	142.1	157.1	1228	0.364	1.41×10^{2}	0.14	0.016	112	0.116	40.3
NY-111	49.8	0.9884	152.4	168.5	1270	0.377	2.42×10^{2}	0.33	0.039	162	0.120	34.4
NY-112	65.6	1.0821	186.4	206.0	1132	0.336	2.70×10^{2}	0.35	0.058	215	0.165	40.5
NY-114	2924	0.0265	129.1	142.6	1165	0.347	1.54×10^{3}	22.7	2.51	1630	0.111	40.0
NY115	249	0.0459	155.0	171.2	948	0.281	1.39×10^{3}	1.61	0.263	189	0.163	41.2
NY-116	787	0.0221	172.2	190.2	818	0.242	1.21×10^{4}	4.57	0.963	79	0.211	48.8
NY-117	769	0.4304	147.5	163.0	7790	0.234	9.40×10^{3}	5.21	0.974	104	0.187	42.9
Owego	136,000	0.0300	763.2	848.0	1416	0.430	1.64×10^{5}	177.9	95.85	584	0.539	34.3
Min	19.4	0.02	85.6	95.2	782	0.231	6.21	0.14	0.016	12	0.065	20.0
Max	136000	1.42	862.5	958.3	4613	1.363	1.64×10^{5}	177.9	95.85	18,388	0.434	52.4
Mean	4916	0.46	267.5	297.5	1367	0.404	7.99×10^{3}	12.77	3.894	2342	0.191	37.3
Standard deviation	16007	0.39	143.9	159.2	501	0.148	2.15×10^{4}	28.69	11.725	3568	0.082	6.7

and fault-associated samples, there is a distinct correlation between elevated [^{4}He] and location with respect to valley bottom ($p = 0.01$). However, we found no significant correlation of dissolved [^{4}He] or ^{4}He/CH_4 with proximity to oil or gas wells ($p = 0.43$).

Atmospheric Noble Gases

Figure 4 demonstrates that most samples with low methane concentrations display ^{20}Ne, ^{36}Ar, and N_2 concentrations close to the air-saturated water (ASW) solubility concentrations (± ~15%) with small additions of excess air (added along the atmospheric vector), as is common in shallow groundwater worldwide (Heaton and Vogel 1981; Solomon et al. 1992; Aeschbach-Hertig et al. 2008). These data are consistent with anticipated ASW values without evidence of gas stripping as has been observed in the NAB near areas with documented gas-well leakage (Darrah et al. 2014).

Unlike the majority of nonfault-associated samples, the subset of high methane, fault-associated samples, displays significant excesses of ^{20}Ne and correspondingly elevated ratios of ^{20}Ne/^{36}Ar, ranging between 0.30 and 0.434 in groundwater samples and up to 0.539 in the Owego brine, or more than twice the solubility ratio (Figure 4; Table 3). Because the ^{20}Ne/^{36}Ar occurs without any significant increase in the ^{36}Ar concentration, we preclude the addition of excess air. A plot of ^{4}He/CH_4 vs. ^{20}Ne/^{36}Ar displays significant scatter, but a correlation between ^{4}He/CH_4 and ^{20}Ne/^{36}Ar in samples with enrichment of ^{20}Ne/^{36}Ar is apparent, specifically in the sample from the Owego brine (black square). Thus, we conclude that excess neon is related to two-phase (gas + brine) fluid migration in the subsurface.

Discussion

Like previous studies, the correlations between thermogenic hydrocarbon gases (i.e., CH_4, C_2H_6), highly elevated, exogenous ^{4}He, excess atmospheric ^{20}Ne, and salts (i.e., Cl, Br, and Ba) suggest that a common process

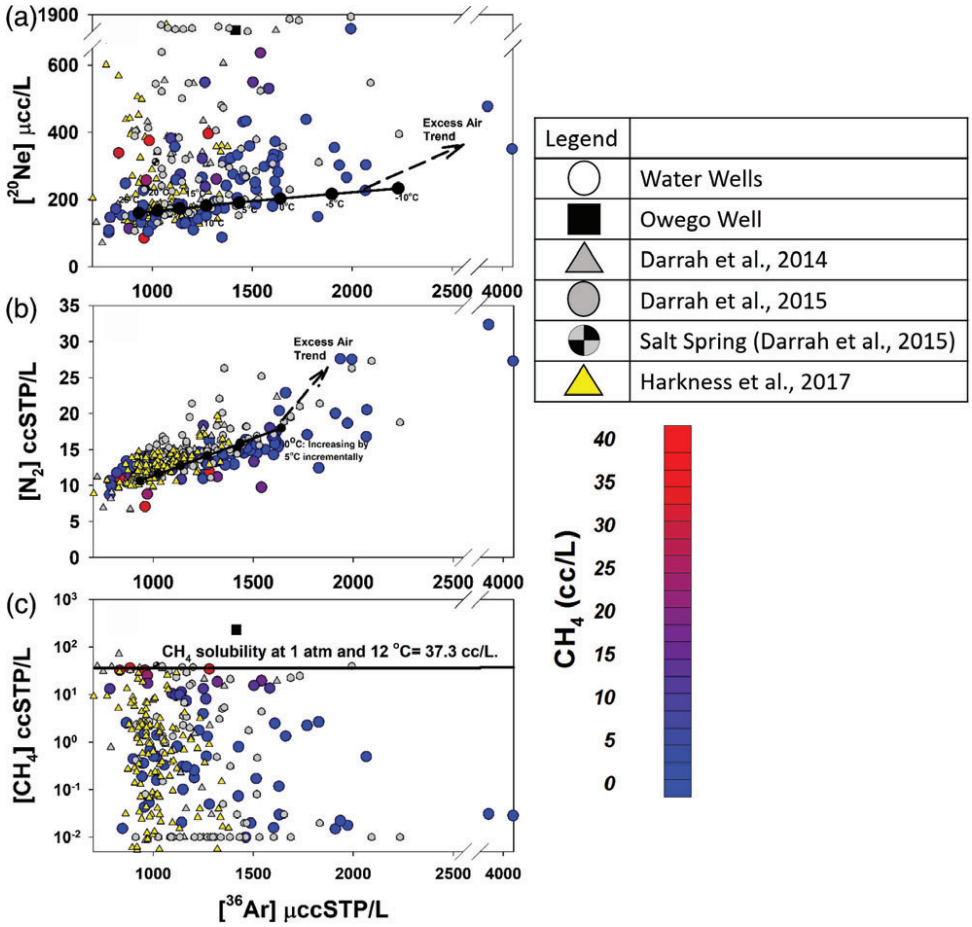

Figure 4. The concentrations of ^{20}Ne (a), N_2 (b), and CH_4 (c) vs. ^{36}Ar in the shallow groundwater and Owego brine samples in the study area compared to previously published groundwater data (gray triangles [Darrah et al., 2013], gray circles [Darrah et al. 2015a], yellow triangles [Harkness et al. 2017]) and a natural salt spring end-member (checkered circle, Darrah et al. 2015b). In natural groundwater aquifers, the concentration of atmospheric (ASW) gases (i.e., N_2, ^{20}Ne, ^{36}Ar) is determined by the solubility of each gas during meteoric recharge. Note that the elevated [^{20}Ne] and ^{20}Ne/^{36}Ar in a subset of methane-rich samples indicate significant two-phase migration during transport to shallow aquifers.

coherently regulates naturally-occurring hydrocarbon gas and salt contamination within shallow aquifers in the southern tier of New York State within the NAB. Here we utilize the levels of each of these parameters to evaluate (1) the occurrence and geochemical character of naturally occurring hydrocarbon gases prior to potential unconventional drilling; (2) the mechanism(s) for the migration of these fluids to shallow aquifers; and (3) the role of faults as pathways for the migration of naturally occurring hydrocarbon gases and salts to shallow aquifers in the NAB.

The Occurrence and Geochemical Character of Naturally Occurring Hydrocarbon Gases

Like the Karoo Basin (discussed in this volume) and other petroleum basins, the complex tectonic and hydrogeological history of the NAB has produced a complex distribution of hydrocarbon sources and fluid migration pathways. Elevated methane concentrations corresponded to samples with elevated levels of salts with a Na-Cl composition (Figure 3; Tables 1 and 2), higher relative ethane levels, markedly higher levels of ^{4}He, and elevated ^{20}Ne/^{36}Ar (Figures 3, 5, 6, 7, and 8). Groundwater samples that exhibited correlations between these components have been attributed previously to the migration of a hydrocarbon-rich brine from source rocks to shallow aquifers over unknown periods of geological time (Warner et al. 2012a, 2012b; Jackson et al., 2013; Darrah et al. 2015b; Eymold et al. 2018). These observations are consistent with other areas in the NAB and around the world (Darrah et al. 2014, 2015a, 2015b; Harkness et al. 2017; Moore et al. 2018; Eymold et al. 2018).

While groundwater from the current study in New York State resembles previous results documented in Pennsylvania, West Virginia, and New York (Heisig and Scott 2013; Darrah et al. 2014, 2015b; Lautz et al. 2014; Harkness et al. 2017), the magnitude of chemical variation is much higher in Pennsylvania groundwater than that in New York. For example, the highest concentrations of helium documented in New York are 37,090 $\times$ 10^{-6} ccSTP/L, which is nearly an order of magnitude lower than Pennsylvania (403,035 $\times$ 10^{-6} ccSTP/L) (Darrah et al. 2014, 2015b). Groundwater samples from Pennsylvania also demonstrate more extensive

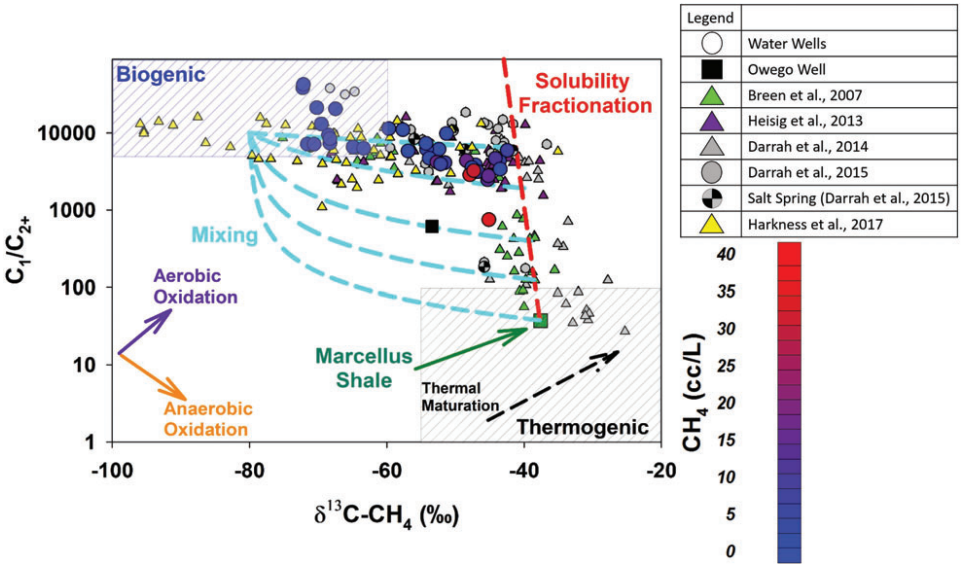

Figure 5. The C_1/C_2+ vs. δ^{13}C-CH$_4$ in groundwater samples and the Owego brine sample from the current study area. We compare our data to published data (green triangles [Breen et al., 2007], purple triangles [Heisig and Scott 2013], gray triangles [Darrah et al., 2013], gray and checkered circles [Darrah et al. 2015b], and yellow triangles [Harkness et al. 2017]) and the values of Marcellus production gases (green box). Notice that many of the groundwater samples do not plot along a simple two-component mixing trajectory between thermogenic and biogenic gases, even if one assumes a relatively enriched microbial end-member (δ^{13}C-CH$_4 = -52$ per mille). When combined with noble gas data, it appears that the trend typified by the rapid depletion of C_2 relative to C_1, previously interpreted as postgenetic fractionation by "diffusional fractionation" (Prinzhofer and Pernaton, 1997), may instead reflect solubility fractionation (red dashed line) during the advection of a dual-phase (water and gas) fluid.

fractionation of the ^{4}He/CH$_4$ and ^{20}Ne/^{36}Ar relative to New York groundwater samples (Figure 7). We preliminarily attribute these trends to differences in basin geometry, a changing structural regime, different liquid/gas ratios, and the extent of vertical fluid migration from the same source horizon (fluids migrated to higher levels in Pennsylvania relative to New York).

Sources of Naturally Occurring Hydrocarbon Gases

Hydrocarbon gas within groundwater can be produced in shallow aquifers by biogenic (via microbes) or thermogenic processes, or result from subsurface migration from an exogenous source of biogenic or thermogenic gas (Darrah et al. 2015a, 2015b). Typically, the source or genetic origin of hydrocarbon gases in shallow aquifers is determined by a combination of the molecular composition of gases (e.g., the ratio of methane [C_1] to higher-order hydrocarbons [C_2+], or C_1/C_2+) and the stable isotopic compositions of methane (e.g., δ^{13}C-CH$_4$).

Data from the present study display a large range of δ^{13}C-CH$_4$ (−79.30 to −34.71‰) with a correspondingly narrow range of C_1/C_2+, especially in the methane-rich end-member (2469 to 8403). The low-methane samples in the upper left-hand corner of Figure 5 display both extremely high C_1/C_2+ and very negative δ^{13}C-CH$_4$ ($\leq \sim$70‰); these samples can be attributed to biogenic sources and demonstrate the presence of a natural background of low-level biogenic methane. In comparison, there is greater uncertainty in interpreting the methane-rich samples that contain higher levels of ethane (leading to C_1/C_2+ ratios between 612 and ~5000) and relatively more enriched carbon isotopes in methane (δ^{13}C-CH$_4 = \sim -50$ to −40‰). The relative increase in ethane concentrations, ^{4}He, elevated ^{20}Ne/^{36}Ar, and δ^{13}C-CH$_4$ document quantifiable thermogenic contributions in the methane-rich end-members. However, as was reviewed elsewhere in this volume (Eymold et al. 2018), the combination of high C_1/C_2+ and intermediate δ^{13}C-CH$_4$ values is inconsistent with any known thermogenic sources of natural gas.

Similar to the interpretation detailed previously (Harkness et al. 2017; Moore et al. 2018; Eymold et al. 2018), we suggest that the simultaneous increases in ethane, ^{4}He, and especially ^{20}Ne/^{36}Ar, which records a history of two-phase fluid migration, in samples with both high C_1/C_2+ and less negative δ^{13}C-CH$_4$ suggest that the thermogenic natural gas in the methane-rich end-members was likely altered by solubility partitioning. While solubility partitioning can dramatically change the C_1/C_2+, it imparts minimal fractionation on the δ^{13}C-CH$_4$. Like shallow methane-rich fluids from other areas in the NAB, the Illinois Basin, and the Karoo Basin, we suggest that this previously ambiguous thermogenic end-member can likely be accounted for by simple two-component mixing between a biogenic end-member and an early maturity thermogenic end-member that previously experienced postgenetic modification (Figures 5 and 7).

Fluid Migration

Noble gases can be used to document the presence of exogenous fluids and evaluate fluid migration processes (Darrah et al. 2014; Hunt et al. 2012). Similar to

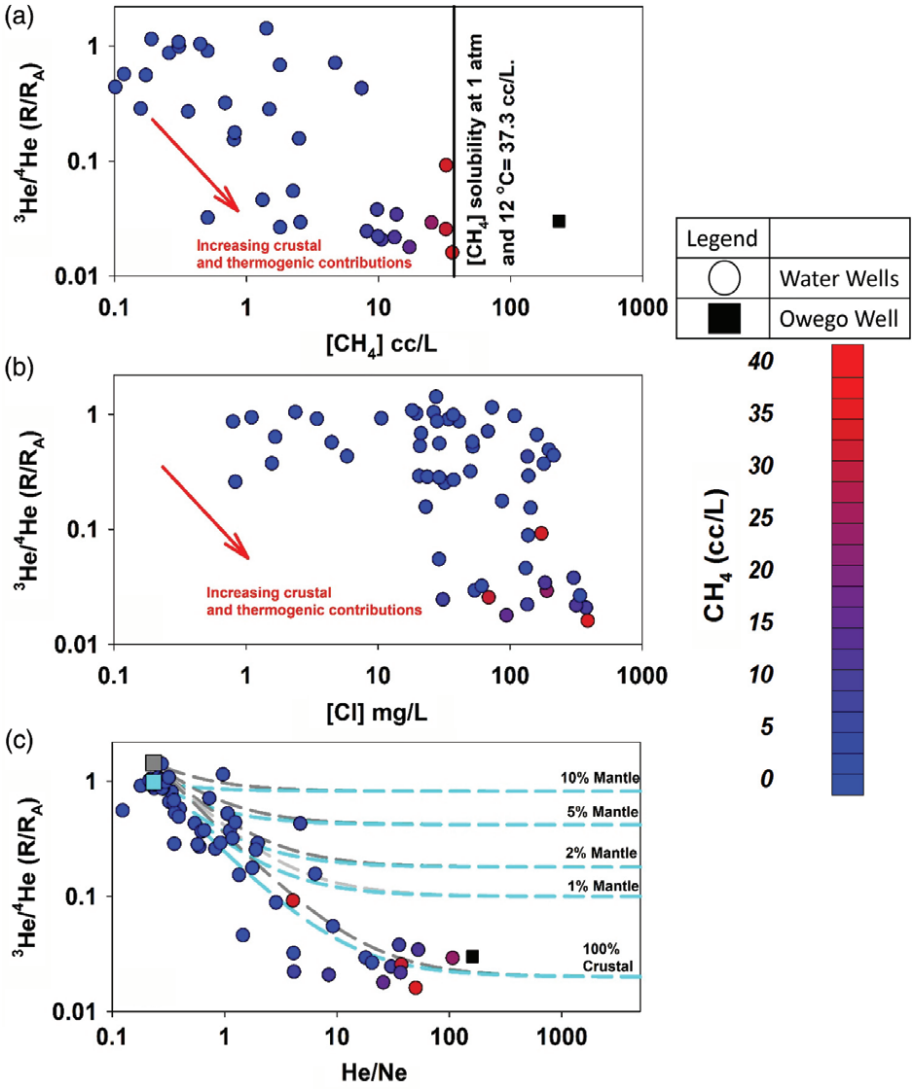

Figure 6. The helium isotopic composition ($^3He/^4He$) shown as the ratio of the sample to air (where the $^3He/^4He$ of air = 1R_A) vs. [CH_4] (a), [Cl] (b), and He/Ne (c) in New York groundwater and the Owego brine. As shown in Figure 6c, the $^3He/^4He$ varies from air-saturated water (light blue box) and tritiated air-saturated water (i.e., ASW enriched in ^3He produced from the radioactive decay of ^3H) (gray box) levels with the additions of crustal ^4He produced from the radioactive decay of U and Th, intrinsic release of ^4He that has accumulated in mineral grains within the aquifer, and a flux from exogenous sources. Our data suggest that the majority of samples have a crustal source of helium, while maximum crustal inputs correspond to the addition of thermogenic natural gas ([CH_4]) (a) and increasingly brine-rich components [Cl] (b).

observations in other basins and other parts of the NAB, the presence of elevated ^4He concentrations up to 37,090 $\times$ 10^{-6} ccSTP/L (~1000 times atmospheric levels) exceeds the viable contributions from ASW, excess air, or the maximum plausible endogenous sources, which confirms the presence of an exogenous helium in a subset of groundwater samples from this study. The correlations between exogenous ^4He, ethane, less negative $\delta^{13}C$-CH_4, elevated $^{20}Ne/^{36}Ar$, and salts (e.g., Cl, Br, Ba) in the methane-rich end-members suggest thermogenic natural gas-rich brine is also likely derived from exogenous sources.

The markedly elevated $^{20}Ne/^{36}Ar$ in the methane-rich samples suggests that an exogenous hydrocarbon-rich brine (from an undetermined source of natural gas in the NAB) migrated to shallow aquifers as a dual-phase fluid. However, the simple addition of a Marcellus or UD production gas (Figures 7 and 8) to shallow groundwater cannot account for this increase in neon because the production gas contains too little neon (e.g., [^{20}Ne] = 30 ppb for Marcellus production gases; 250 ppb for UD production gases (Hunt et al. 2012)) with a lower $^{20}Ne/^{36}Ar$ ratio. To increase the neon to levels observed in the high methane water samples, the added neon-rich component must have about 100$\times$ more neon relative to methane, or about 5 to 10 ppm neon in the gas and a $^{20}Ne/^{36}Ar > 0.5$. The simplest explanation for the high $^{20}Ne/^{36}Ar$ is that solubility fractionation during two-phase (liquid + gas) migration can enrich the migrating natural gas in ^{20}Ne by stripping a sufficient volume of ^{20}Ne relative to ^{36}Ar from groundwater. Numerical modeling suggests that neon can be suitably enriched during gas-phase migration through

the water-saturated crust as was documented in previous reports (Darrah et al. 2014, 2015a, 2015b; Harkness et al. 2017; Moore et al. 2018; Eymold et al. 2018).

Thus, our ad hoc interpretation of the geochemical data suggests that hydrocarbon-gases and brines have likely undergone a two-stage migration that includes: (1) solubility fractionation during dual-phase advection from source to hydrocarbon reservoirs, which is likely followed by (2) secondary stages of fluid transport from incompetent hydrocarbon reservoirs to shallow aquifers, which has previously been suggested to occur by diffusion (Darrah et al. 2014; Harkness et al. 2017).

The Role of Faults in Focusing Hydrocarbon-Rich Brine Migration to Shallow Aquifers

Our results document significant correlations between groundwater that contains elevated levels of naturally occurring hydrocarbon gases, salts, exogenous ^{4}He, and noble gas evidence for extensive migration of these fluids from exogenous sources (i.e., elevated $^{4}He/^{20}Ne$, $^{20}Ne/^{36}Ar$, and $^{4}He/CH_4$). These results are consistent with prior observations around the NAB, the Dallas-Fort Worth Basin, and the Karoo Basin (South Africa) (Warner

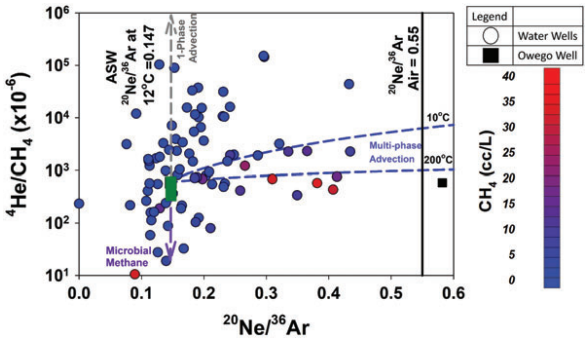

Figure 7. The $^{4}He/CH^{4}$ vs. $^{20}Ne/^{36}Ar$ in dissolved gas in groundwater samples as compared to Marcellus production gas (solid green box). The observed $^{20}Ne/^{36}Ar$ and $^{4}He/CH_4$ data of shallow groundwater are not consistent with one-phase advection, solubility fractionation during advection of a two-phase fluid, or primary diffusion alone. We hypothesize two sequential stages of hydrocarbon-rich brine migration including: (1) transport of the Marcellus gas to UD reservoirs via primary and later secondary (buoyant) migration, during which isotopic fractionation is induced by differential solubility of the gases and (2) a final secondary diffusion of the UD gas into the shallow UD aquifers by tertiary migration.

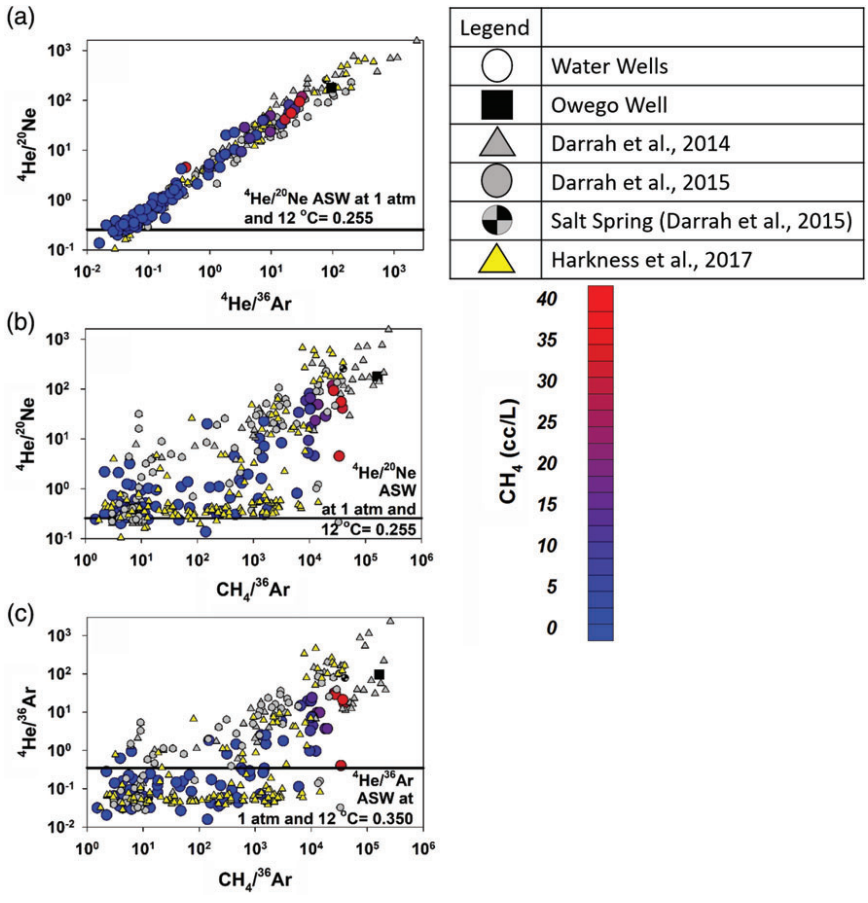

Figure 8. The $^{4}He/^{20}Ne$ vs. $^{4}He/^{36}Ar$ (a), $^{4}He/^{20}Ne$ vs. $CH_4/^{36}Ar$ (b), and $^{4}He/^{36}Ar$ vs. $CH_4/^{36}Ar$ (c) in groundwater samples and the Owego brine sample from the current study. We compare our data to published data (gray triangles [Darrah et al., 2014], gray and checkered circles [Darrah et al. 2015a], and yellow triangles [Harkness et al. 2017]). The trends of increasing $^{4}He/^{36}Ar$ and $^{4}He/^{20}Ne$ vs. $CH_4/^{36}Ar$ show a dilution of ^{4}He-rich and CH_4– saturated, salty groundwater by meteoric water with air-saturated water composition. These findings suggest that hydrocarbon-rich brine components were mixed with relatively young meteoric waters in the shallow subsurface.

et al. 2012a; Jackson et al. 2013; Darrah et al. 2014, 2015a, 2015b; Harkness et al. 2017; Moore et al. 2018; Eymold et al. 2018). The novel observation documented as part of this study is the spatial relationship between the presence of elevated levels of these tracers in shallow aquifers and proximity to faults in this region of the NAB (Figure 2). Thus, although we recognize that there is often an overlap between samples classified as "valley bottoms" and samples classified as "fault associated," we suggest that faults in the NAB likely provide a pathway for the migration of hydrocarbon-rich brines on undetermined geological time scales.

Obviously, this hypothesis needs additional testing. However, if faults control the migration of hydrocarbon-rich brines to shallow aquifers, one must conclude that the migration of hydrocarbon-rich brines is not ubiquitous throughout the basin and that hydrodynamic focusing of methane and brine to valley bottoms is not the dominant process controlling elevated levels of these natural contaminants in shallow aquifers in the region. Instead, these results suggest that methane and salt contamination occur along localized, discrete faults, which may have been active since at least the time of Alleghanian orogeny. Further, if subsequent analysis demonstrates that faults *do* control the migration of hydrocarbon-rich brines to shallow aquifers, future work should include efforts toward fault identification during seismic surveys and detailed geological field observations when developing groundwater risk assessments for potential methane and salt contamination.

Conclusions

The combination of traditional hydrocarbon gas (molecular and isotopic composition), noble gas, and dissolved ion geochemistry provides important insights on the occurrence and processes that control naturally occurring methane- and salt-contamination in shallow aquifers overlying the Marcellus Shale in the southern tier of New York State in the NAB. Like previous studies from other petroliferous basins, our results show significant correlations between elevated levels of radiogenic [^{4}He], thermogenic [CH_4], and dissolved ions (e.g., Cl, Br, Sr, Ba). In combination, these data suggest that thermogenic methane and salts were generated in exogenous formations and migrated to overlying UD aquifer lithologies over geologic time. In apparent contrast to previous hypotheses that evoke hydrodynamic focusing in valley bottoms as the dominant mechanism that regulates the occurrence of methane and salt in shallow aquifers, our data suggest that faults in UD aquifer lithologies play a fundamental role in gas and brine transport from depth, regulate the distribution of their occurrence in shallow aquifers, and influence the geochemistry of shallow groundwater in this petroliferous basin. Because there is significant overlap between valley bottoms and fault-associated areas, future work should further test this theory in diverse tectonic and hydrogeological settings.

Authors' Note

The author(s) does not have any conflicts of interest or financial disclosures to report.

Acknowledgments

We would like to acknowledge financial support from NSF EAGER (EAR-1249255) and NSF SusChem (EAR-1441497) to T.H.D, A.V.,and R.B.J.

References

Aeschbach-Hertig, W., H. El-Gamal, M. Wieser, and L. Palcsu. 2008. Modeling excess air and degassing in groundwater by equilibrium partitioning with a gas phase. *Water Resources Research* 44, no. 8: 1–12.

Baldassare, F.J., M.A. McCaffrey, and J.A. Harper. 2014. A geochemical context for stray gas investigations in the northern Appalachian Basin: Implications of analyses of natural gases from neogene-through Devonian-age strata. *AAPG Bulletin* 98, no. 2: 341–372.

Brantley, S.L., D. Yoxtheimer, S. Arjmand, P. Grieve, R. Vidic, J. Pollak, G.T. Llewellyn, J. Abad, and C. Simon. 2014. Water resource impacts during unconvetional shale gas development: The Pennsylvania experience. *International Journal of Coal Geology* 126: 140–156.

Breen, K.J., K. Revesz, F.J. Baldassare, and S.D. McAuley. 2007. Natural gases in ground water near Tioga Junction, Tioga County, North-Central Pennsylvania-Occurrence and Use of Isotopes to Determine Origins, 2005. U.S. Geological Survey Scientific Investigations Report 2007-5085. Reston, Virginia: USGS.

Burruss, R.C., and C.D. Laughrey. 2010. Carbon and hydrogen isotopic reversals in deep basin gas: Evidence for limits to the stability of hydrocarbons. *Organic Geochemistry* 41, no. 12: 1285–1296.

Caine, S.C., J.P. Evans, and C.B. Forster. 1996. Fault zone architecture and permeability structure. *Geology* 24, no. 11: 1025–1028.

Dahlstrom, C.D.A. 1970. Structural geology in the easter margin of the Canadian Rocky Mountains. *Bulletin of Canadian Petroleum Geology* 18: 332–406.

Darrah, T.H. 2018. Time to settle the fracking controversy. *Groundwater* 56, no. 2: 1–2.

Darrah, T.H., and R.J. Poreda. 2012. Evaluating the accretion of meteoritic debris and interplanetary dust particles in the GPC-3 sediment core using noble gas and mineralogical tracers. *Geochimica et Cosmochimica Acta* 84: 329–352.

Darrah, T.H., D. Tedesco, F. Tassi, O. Vaselli, E. Cuoco, and R.J. Poreda. 2013. Gas chemistry of the Dallol region of the Danakil depression in the afar region of the northern-most east African rift. *Chemical Geology* 339: 16–29.

Darrah, T., A. Vengosh, R.B. Jackson, N.R. Warner, and R.J. Poreda. 2014. Noble gases identify the mechanisms of fugitive gas contamination in drinking-water wells overlying the Marcellus and Barnett shales. *Proceedings of the National Academy of Sciences of the United States of America* 111, no. 39: 14076–14081.

Darrah, T.H., R.B. Jackson, A. Vengosh, N.R. Warner, and R.J. Poreda. 2015a. Noble gases: A new technique for fugitive gas investigation in groundwater. *Groundwater* 53, no. 1: 23–28.

Darrah, T.H., R.B. Jackson, A. Vengosh, N.R. Warner, C.J. Whyte, T.B. Walsh, A.J. Kondash, and R.J. Poreda. 2015b. The evolution of Devonian hydrocarbon gases in shallow aquifers of the northern Appalachian Basin: Insights from integrating noble gas and hydrocarbon geochemistry. *Geochimica et Cosmochimica Acta* 170: 321–355.

David, G., T.E. Lombardi, and J.P. Martin. 2004. Fractured shale gas potential in New York. *Northeastern Geology and Environmental Sciences* 26, no. 1/2: 57–78.

Drozd, R.J., and G.A. Cole. 1994. Point pleasant-Brassfield petroleum system, Appalachian basin, U.S.A. In *The Petroleum System - From Source to Trap*, Vol. 60, ed. L.B. Magoon and W.G. Dow, 387–398. Tulsa, Oklahoma: American Association of Petroleum Geologists Memoir.

Engelder, T., G.G. Lash, and R.S. Uzcategui. 2009. Joint sets that enhance production from middle and upper Devonian gas shales of the Appalachian Basin. *AAPG Bulletin* 93, no. 7: 857–889.

Evans, M.A. 1995. Fluid inclusions in veins from the middle Devonian shales- A record of deformation conditions and fluid evolution in the Appalachian plateau. *Geological Society of America Bulletin* 107, no. 3: 327–339.

Eymold, W.K., K. Swana, M.T. Moore, C.J. Whyte, J.S. Harkness, S. Talma, J. Moortgat, R. Murray, A. Vengosh, and T.H. Darrah. 2018. Hydrocarbon-rich groundwater above shale-gas formations: A Karoo Basin case-study. *Groundwater* 56, no. 2.

Faill, R.T., and R.P. Nickelsen. 1973. Structural geology. Structure and Silurian-Devonian stratigraphy of the Valley and Ridge province, central Pennsylvania. Paper presented at 38th Field Conference of Pennsylvania Geologists, Harrisburg, Pennsylvania, 9–38.

Fettke, C.R. 1954. *Struture-Contour Maps of the Plateau Region of North-Central and Western Pennsylvania*. Harrisburg, Pennsylvania: Pennsylvania Bureau of Topographic and Geologic Survey.

Finn, F.H. 1949. Geology and occurrence of natural gas in Oriskany sandstone in Pennsylvania and New York. *American Association of Petroleum Geologists Bulletin* 33, no. 3: 303–335.

Frey, M.G. 1973. Influence of Salina salt on structure in New York-Pennsylvania part of the Appalachian plateau. *American Association of Petroleum Geologists Bulletin* 57, no. 6: 1027–1037.

Gwinn, V.E. 1964. Thin-skinned tectonics in the plateau and northwestern valley and ridge provinces of the central Appalachians. *Geological Society of America Bulletin* 75: 863–900.

Harkness, J.S., T.H. Darrah, N.R. Warner, C.J. Whyte, M.T. Moore, R. Millot, W. Kloppmann, R.B. Jackson, and A. Vengosh. 2017. The geochemistry of naturally occurring methane and saline groundwater in an area of unconventional shale gas development. *Geochimica et Cosmochimica Acta* 208: 302–334.

Harkness, J.S., K. Swana, W.K. Eymold, J. Miller, R. Murray, S. Talma, C.J. Whyte, M.T. Moore, E.L. Maletic, A. Vengosh, and T.H. Darrah. 2018. Baseline groundwater geochemistry in the Karoo Basin, South Africa. *Groundwater* 56, no. 2.

Hatcher, R.D., W.A. Thomas, P. Geiser, A.W. Snoke, and D.V. Wiltschko. 1989. *Alleghanian Orogen*, Vol. F-2. Boulder, Colorado: Geological Society of America.

Heaton, T.H.E., and J.C. Vogel. 1981. Excess air in groundwater. *Journal of Hydrology* 50, no. 1–3: 201–216.

Heilweil, V.M., P.L. Grieve, S.A. Hynek, S.L. Brantley, D.K. Solomon, and D.W. Risser. 2015. Stream measurements locate thermogenic methane fluxes in groundwater discharge in an area of shale-gas development. *Environmental Science & Technology* 49, no. 7: 4057–4065.

Heisig, P.M., and T.M. Scott. 2013. *Methane Occurrence in Groundwater of South-Central New York State, 2012-Systematic Evaluation of a Glaciated Region by Hydrogeologic Setting*. Reston, Virginia: U.S. Geological Survey.

Hill, D.G., and T.E. Lombardi. 2002. *Fractured Gas Shale Potential in New York*. Arvada, Colorado: Colorado Publishing.

Humez, P., B. Mayer, J. Ing, M. Nightingale, V. Becker, A. Kingston, O. Akbilgic, and S. Taylor. 2016. Occurrence and origin of methane in groundwater in Alberta (Canada): Gas geochemical and isotopic approaches. *Science of the Total Environment* 541: 1253–1268.

Hunt, A.G., T.H. Darrah, and R.J. Poreda. 2012. Determining the source and genetic fingerprint of natural gases using noble gas geochemistry: A northern Appalachian Basin case study. *AAPG Bulletin* 96, no. 10: 1785–1811.

Isotech. 2011. *Collection of Groundwater Samples from Domestic and Municipal Water Wells for Dissolved Gas Analysis*. Champaign, Illinois: Isotech.

Jackson, R.B., A. Vengosh, T.H. Darrah, N.R. Warner, A. Down, R.J. Poreda, S.G. Osborn, K. Zhao, and J.D. Karr. 2013. Increased stray gas abundance in a subset of drinking water wells near Marcellus shale gas extraction. *Proceedings of the National Academy of Sciences of the United States of America* 110, no. 28: 11250–11255.

Jacobi, R.D. 2002. Basement faults and seismicity in the Appalachian Basin of New York state. *Tectonophysics* 353, no. 1: 75–113.

Jacoby, C.H., and L. Dellwig. 1974. Appalachian foreland thrusting in salina salt, Watkins Glen, New York. Paper presented at 4th International Symposium on Salt, Northern Ohio Geological Society, Inc, Cleveland, Ohio.

Kang, M., S. Christian, M.A. Celia, D.L. Mauzerall, M. Bill, A.R. Miller, Y. Chen, M.E. Conrad, T.H. Darrah, and R.B. Jackson. 2016. Identification and characterization of high methane-emitting abandoned oil and gas wells. *Proceedings of the National Academy of Sciences of the United States of America* 113, no. 48: 13636–13641.

Lash, G.G., and T. Engelder. 2009. Tracking the burial and tectonic history of Devonian shale of the Appalachian Basin by analysis of joint intersection style. *Geological Society of America Bulletin* 121, no. 1–2: 265–277.

Lautz, L.K., G.D. Hoke, Z. Lu, D.I. Siegel, K. Christian, J.D. Kessler, and N.G. Teale. 2014. Using discriminant analysis to determine sources of salinity in shallow groundwater prior to hydraulic fracturing. *Environmental Science & Technology* 48, no. 16: 9061–9069.

Lerche, I., Z. Yu, B. Tørudbakken, and R. Thomsen. 1997. Ice loading effects in sedimentary basins with reference to the Barents Sea. *Marine and Petroleum Geology* 14, no. 3: 277–338.

Milici, R.C., and W.D. Witt. 1988. The Appalachian Basin. In *The Geology of North America*, ed. L.L. Sloss, 427–469. Denver, Colorado: GSO America.

Miller, T., and L. Pitman. 2012. Hydrogeology of the stratified-drift aquifers in the Cayuta Creek and Catatonk Creek valleys in parts of Tompkins. Schuyler, Chemung, and Tioga counties, New York. *US Geological Survey Scientific Investigations Report* 5127, no. 44: 3.

Mitra, S. 2002. Fold-accommodation faults. *AAPG Bulletin* 86, no. 4: 671–694.

Molofsky, L.J., J.A. Connor, A.S. Wylie, T. Wagner, and S.K. Farhat. 2013. Evaluation of methane sources in groundwater in northeastern Pennsylvania. *Groundwater* 51, no. 3: 333–349.

Moore, M.T., D.S. Vinson, C.J. Whyte, W.K. Eymold, T.B. Walsh, and T.H. Darrah. 2018. Differentiating between biogenic and thermogenic sources of natural gas in coalbed methane reservoirs from the Illinois Basin using noble gas and hydrocarbon geochemistry. In *From Source to Seep: Geochemical Applications in Hydrocarbon Systems*, ed. M. Lawson, M.J. Formolo, and J.M. Eiler. Special Publications 468–505. London: Geological Society. https://doi.org/10.1144/SP468.8

Moritz, A., J.F. Hélie, D.L. Pinti, M. Larocque, D. Barnetche, S. Retailleau, R. Lefebvre, and Y. Gélinas. 2015. Methane baseline concentrations and sources in shallow aquifers from teh shale gas-prone region of the St. Lawrence lowlands (Quebec, Canada). *Environmental Science & Technology* 49, no. 7: 4765–4771.

Murphy, P.J. 1981. Detachment structures in south-central New York. *Northeastern Geology* 3: 105–116.

Nicot, J.P., T. Larson, R. Darvari, P. Mickler, M. Slotten, J. Aldridge, K. Uhlman, and R. Costley. 2017a. Controls on methane occurrences in shallow aquifers overlying the Haynesville shale gas field, East Texas. *Groundwater* 55, no. 4: 443–454.

Nicot, J.P., T. Larson, R. Darvari, P. Mickler, K. Uhlman, and R. Costley. 2017b. Controls on methane occurrences in aquifers overlying the eagle ford shale play, South Texas. *Groundwater* 55, no. 4: 455–468.

Nicot, J.P., P. Mickler, T. Larson, M. Clara Castro, R. Darvari, K. Uhlman, and R. Costley. 2017c. Methane occurrences in aquifers overlying the Barnett shale play with a focus on Parker County, Texas. *Groundwater* 55, no. 4: 469–481.

Osborn, S.G., A. Vengosh, N.R. Warner, and R.B. Jackson. 2011. Methane contamination of drinking water accompanying gas-well drilling and hydraulic fracturing. *Proceedings of the National Academy of Sciences of the United States of America* 108, no. 20: 8172–8176.

Prinzhofer, A., and É. Pernaton. 1997. Isotopically light methane in natural gas: Bacterial imprint or diffusive fractionation? *Chemical Geology* 142, no. 3: 193–200.

Repetski, J.E., R.T. Ryder, D.J. Weary, A.G. Harris, and M.H. Trippi. 2008. Thermal maturity patterns (CAI and% Ro) in Upper Ordovician and Devonian rocks of the Appalachian basin: A major revision of USGS Map I-917-E using new subsurface collections. Reston, Virginia: US Geological Survey.

Rodgers, J. 1949. Evolution of thought on structure of middle and southern Appalachians. *AAPG Bulletin* 33, no. 10: 1643–1654.

Ryder, R.T., and W.A. Zagorski. 2003. Nature origin and production characteristics of the lower Silurian regional oil and gas accumulation, central Appalachian basin, United States. *AAPG Bulletin* 87, no. 5: 847–872.

Ryder, R.T., K.L. Aggen, R.D. Hettinger, B.E. Law, J.J. Miller, V.F. Nuccio, W.J. Perry, S.E. Prensky, J.R. SanFilipo, and C.J. Wandry. 1996. Possible continuous-type (unconventional) gas accumulation in the Lower Silurian "Clinton" sands, Medina Group, and Tuscarora Sandstone in the Appalachian basin: A progress report of 1995 activities. USGS Open-File Report 96-42. Denver, Colorado: U.S. Geological Survey.

Ryder, R.T., R.C. Burruss, and J.R. Hatch. 1998. Black shale source rocks and oil generation in the Cambrian and Ordovician of the central Appalachian Basin, USA. *AAPG Bulletin* 82, no. 3: 412–441.

Scanlin, M.A., and T. Engelder. 2003. The basement versus the no-basement hypotheses for folding within the Appalachian plateau detachment sheet. *American Journal of Science* 303, no. 6: 519–563.

Sherwood, O.A., J.D. Rogers, G. Lackey, T.L. Burke, S.G. Osborn, and J.N. Ryan. 2016. Groundwater methane in relation to oil and gas development and shallow coal seams in the Denver-Julesburg Basin of Colorado. *Proceedings of the National Academy of Sciences of the United States of America* 113, no. 30: 8391–8396.

Siegel, D.I., N.A. Azzolina, B.J. Smith, A.E. Perry, and R.L. Bothun. 2015. Methane concentrations in water wells unrelated to proximity to existing oil and gas wells in northeastern Pennsylvania. *Environmental Science & Technology* 49, no. 7: 4106–4112.

Solomon, D.K., R.J. Poreda, S.L. Schiff, and J.A. Cherry. 1992. Tritium and he-3 as groundwater age tracers in the Borden aquifer. *Water Resources Research* 28, no. 3: 741–755.

Straeten, C.A.V., C.E. Brett, and B.B. Sageman. 2011. Mudrock sequence stratigraphy: A multi-proxy (sedimentological, paleobiological and geochemical) approach, Devonian Appalachian Basin. *Palaeogeography Palaeoclimatology Palaeoecology* 304, no. 1–2: 54–73.

Taylor, L. 1984. Groundwater Resources of the Upper Susquehanna River Basin, Pennsylvania. Water Resources Report 58. Harrisburg, Pennsylvania: Pennsylvania Department of Environmental Resources-Office of Parks and Forestry – Bureau of Topographic and Geologic Survey.

USGS. 2011. *National Field Manual for the Collection of Water-Quality Data*. Washington, DC: USGS.

Vengosh, A., R.B. Jackson, N. Warner, T.H. Darrah, and A. Kondash. 2014. A critical review of the risks to water resources from unconventional shale gas development and hydraulic fracturing in the United States. *Environmental Science & Technology* 48, no. 15: 8334–8348.

Warner, N.R., R.B. Jackson, T.H. Darrah, S.G. Osborn, A. Down, K. Zhao, A. White, and A. Vengosh. 2012a. Geochemical evidence for possible natural migration of Marcellus formation brine to shallow aquifers in Pennsylvania. *Proceedings of the National Academy of Sciences of the United States of America* 109, no. 30: 11961–11966.

Warner, N.R., R.B. Jackson, T.H. Darrah, S.G. Osborn, A. Down, K. Zhao, A. White, and A. Vengosh. 2012b. Reply to Engelder: Potential for fluid migration from the Marcellus formation remains possible. *Proceedings of the National Academy of Sciences of the United States of America* 109, no. 52: E3626–E3626.

Warner, N.R., T.M. Kresse, P.D. Hays, A. Down, J.D. Karr, R.B. Jackson, and A. Vengosh. 2013. Geochemical and isotopic variations in shallow groundwater in areas of the Fayetteville shale development, north-central Arkansas. *Applied Geochemistry* 35: 207–220.

Warner, N.R., T.H. Darrah, R.B. Jackson, R. Millot, W. Kloppmann, and A. Vengosh. 2014. New tracers identify hydraulic fracturing fluids and accidental releases from oil and gas operations. *Environmental Science & Technology* 48, no. 21: 12552–12560.

Wedel, A.A. 1932. Geologic structure of the Devonian strata of south-central New York. *New York State Museum Bulletin* 294. 74 pp.

Wen, T., M.C. Castro, J.P. Nicot, C.M. Hall, T. Larson, P.J. Mickler, and R. Darvari. 2016. Methane sources and migration mechanisms in shallow groundwaters in Parker and Hood Counties, Texas- A heavy noble gas analysis. *Environmental Science & Technology* 50, no. 21: 12012–12021.

Williams, J.H., L.E. Taylor, and D.J. Low. 1998. Hydrogeology and groundwater quality of the glaciated valleys of Bradford, Tioga, and Potter Counites, Pennsylvania. Water Resource Report 68. Denver, Colorado: U.S. Geological Survey.